Article:
Robinson, JI orcid.org/0000-0001-5425-7520, Baxter, EW, Owen, RL et al. (13 more authors) (2018) Affimer proteins inhibit immune complex binding to FcγRIIIa with high specificity through competitive and allosteric modes of action. Proceedings of the National Academy of Sciences, 115 (1). E72-E81. ISSN 0027-8424

https://doi.org/10.1073/pnas.1707856115

Affimer proteins inhibit immune complex binding to FcγRIIIa with high specificity through competitive and allosteric modes of action.

Authors

James I Robinson[1], Euan W Baxter[1•], Robin L Owen[2•], Maren Thomsen[3•], Darren C Tomlinson[3,4•], Mark P. Waterhouse[1•], Stephanie J Win[1], Joanne E Nettleship[5], Christian Tiede[3], , Richard J Foster[4,6], Raymond J Owens[5], Colin WG Fishwick[4,6], Sarah A. Harris[4,7], Adrian Goldman[3,8], Michael J McPherson[3,4], Ann W Morgan[1]

[1]Leeds Institute of Rheumatic and Musculoskeletal Medicine, School of Medicine, University of Leeds, LS9 7TF and NIHR- Leeds Musculoskeletal Biomedical Research Centre, Leeds Teaching Hospitals NHS Trust

[2]Diamond Light Source, Harwell Science and Innovation Campus, Didcot OX11 0DE

[3]BioScreening Technology Group, School of Molecular and Cellular Biology, University of Leeds, LS2 9JT

[4]Astbury Centre for Structural and Molecular Biology, University of Leeds, LS2 9JT

[5]Oxford Protein Production Facility-UK, Research Complex at Harwell, Rutherford Appleton Laboratory, Oxford OX11 0FA and Division of Structural Biology, Henry Wellcome Building for Genomic Medicine OX3 7BN

[6]School of Chemistry, University of Leeds, LS2 9JT

[7]School of Physics and Astronomy, University of Leeds, LS2 9JT

[8]Faculty of Biological and Environmental Sciences, PO Box 65, University of Helsinki, FIN-0014, Helsinki, Finland

• Contributed equally to this work and should be considered joint second authors.

Correspondence should be addressed to Professor Ann W Morgan, Leeds Institute of Rheumatic and Musculoskeletal Medicine, Wellcome Trust Brenner Building, St James's University Hospital, School of Medicine, University of Leeds, LS9 7TF or Professor Michael McPherson, BioScreening Technology Group, School of Molecular and Cellular Biology, University of Leeds, LS2 9JT

e-mail: a.w.morgan@leeds.ac.uk; m.j.mcpherson@leeds.ac.uk

Telephone 44(0)113 343 8414 / 44(0)113 343 2595

ABSTRACT

Protein-protein interactions are essential for the control of cellular functions and critical for regulation of the immune system. One example is the binding of Fc regions of immunoglobulin G (IgG) to the Fc gamma receptors (FcγRs). High sequence identity (98%) between the genes encoding FcγRIIIa (expressed on macrophages and NK cells) and FcγRIIIb (expressed on neutrophils) has prevented development of monospecific agents against these therapeutic targets. We now report the identification of FcγRIIIa-specific artificial binding proteins called ”Affimer” that block IgG binding and abrogate FcγRIIIa-mediated downstream effector functions in macrophages, namely TNF release and phagocytosis. Cocrystal structures and molecular dynamics simulations have revealed the structural basis of this specificity for two Affimer proteins: One binds directly to the Fc binding site, whereas the other acts allosterically.

SIGNIFICANCE STATEMENT

Autoimmune disease pathogenesis is driven by inflammation, induced partly by IgG autoantibody-containing immune complexes binding to Fc gamma receptors (FcγRs). These receptors are widely considered to be valid therapeutic targets in the treatment of autoimmunity. FcγRIIIa is one of a family of highly homologous receptors for IgG antibodies; previous attempts at therapeutic blockade have resulted in off-target effects involving cells which express the almost identical protein FcγRIIIb. Here we report the identification of functionally specific protein-based inhibitors (Affimer proteins) of FcγRIIIa and the structural/functional basis of their selectivity. As molecular research tools FcγRIIIa-specific Affimer proteins provide the ability to block IgG interaction with a single receptor. Our findings suggest that highly selective protein-based blocking agents that may have therapeutic applications can be readily produced.

/body

Improved understanding of genetic, genomic and cellular processes underpinning human disease have led to the identification of a multitude of protein-protein interactions that represent potentially important therapeutic targets, frequently for multiple diseases. Drug discovery has traditionally focused on classical enzyme pockets, and chemical libraries are screened to identify inhibitors using biochemical and biophysical assays. Protein-protein interactions are notoriously difficult to target by this approach, since the interfaces frequently comprise large contact surfaces, which generally lack the deep pockets required for traditional medicinal chemistry approaches. In recent years, alternative strategies have emerged including fragment-based approaches to explore the chemical space or the use of peptide-based recognition molecules, such as hydrocarbon-stapled peptides, alpha mimetics, non-antibody protein scaffolds and antibody-aided technologies (reviewed in (1)). Proteomimetic molecules have inherently greater potential to bind to critical interaction interfaces and sterically block protein-protein interactions. Traditional computational-based design tools have tended to focus on orthosteric inhibitors that directly target the interaction site, such as the receptor ligand-binding domain or active site of an enzyme. Novel approaches for therapeutic development include stabilization of protein complexes and identification of allosteric modulators that bind at sites distant to the interacting proteins (2, 3).

Currently, antibodies are the best-studied group of protein-based inhibitors with a wide range of therapeutic humanized monoclonal antibodies already in clinical use (4). However, antibodies are not always ideal as molecular tools due to their multiple domains and chains, poor stability, high production costs and batch-to-batch variation, some of which may be due to glycosylation heterogeneity (5). Artificial binding reagents (protein, RNA and DNA aptamers) are relatively small and make attractive alternatives to antibodies. We have recently established a scaffold consensus protein based on plant cystatins, called “Affimer”, also known as “Adhiron” (12 kDa), which provides a highly stable scaffold (melting temperature = 101°C) for presenting one to three variable amino acid sequence regions for molecular recognition (6). These variable regions (VRs) form a binding interface analogous to that presented by the complementarity-determining regions of an antibody. Affimer proteins are selected from phage display libraries (>$3x10^{10}$) allowing rapid identification of highly specific reagents that selectively bind to a target and often act as competitive or allosteric inhibitors (7-9). Non-antibody binding proteins tend to recognize binding ‘hot spots’, which are small groups of amino acids on the target protein that contribute the majority of the interaction free energy (10). We propose that Affimer proteins can be used to study protein function and to disrupt protein-ligand interactions. This unbiased approach may also increase the potential for introducing selectivity where multiple receptors bind to a single

ligand, or conversely where multiple ligands bind to a single receptor. We have explored the potential utility of this approach using human Fcγ Receptors (FcγRs) as a model system.

Human FcγR-ligand interactions constitute a biological system whereby multiple layers of complexity facilitate the fine-tuning of immune responses to infections. Immunoglobulin G (IgG) is the major ligand and mediates both pro- and anti-inflammatory effects following immune complex formation and engagement with different FcγRs. These activating and inhibitory receptors play a central role in the initiation and regulation of many immunological processes, including setting thresholds for B cell activation, recruitment of leukocytes, proinflammatory mediator release, phagocytosis and antibody-dependent cellular cytotoxicity (ADCC) (11, 12). Our genetic studies have demonstrated a number of independent associations with genes in the *FCGR* locus in different autoimmune and inflammatory diseases (13-15). We have also described higher levels of FcγRIIIa on circulating $CD14^{++}$ monocytes in rheumatoid arthritis patients compared with healthy controls, which was correlated with increased TNF release on exposure to immune complexes and inferior treatment outcomes (16). Animal models also provide a strong rationale for targeting FcγRs in autoantibody-mediated inflammatory diseases, including autoantibody/immune complex-induced arthritis (17, 18).

There are six functional human FcγRs subdivided into three classes (FcγRI, FcγRIIa, FcγRIIb, FcγRIIc, FcγRIIIa and FcγRIIIb). Multiple segmental duplications and deletions during hominid evolution have resulted in a family of highly homologous receptors with significant divergence of biological functions from those observed in rodents (19, 20). The level of homology has been a major obstacle for the development of FcγR-specific therapeutics.

A number of FcγR class-specific monoclonal antibodies have been tested in humans, predominantly to block ADCC in immune thrombocytopenia purpura (ITP) (21). An antibody against FcγRIII (CD16-3G8) led to transient increases in platelet count, demonstrating early efficacy. However, in addition to immunogenicity, a number of infusion and atypical hypersensitivity reactions were observed in conjunction with neutrophil and monocyte cytopenias that led to early termination of this program. Although these were believed to be secondary to unwanted engagement of the therapeutic Fc region with FcγRs, these were not abrogated when a humanised anti-FcγR with an aglycosylated Fc was used, suggesting alternative approaches may be required (reviewed in (22)). Blockade of the critical proximal signalling molecule spleen tyrosine kinase (SYK) downstream of several FcγRs initially showed promising efficacy in rheumatoid arthritis (23), chronic lymphocytic leukemia and

non-Hodgkin's lymphoma (24), providing clinical support for therapeutic FcγR blockade in human disease. However, further development in rheumatoid arthritis has been suspended, principally due to adverse off-target events (25).

In this proof of principle study, we have screened artificial binding protein libraries against a recombinant, glycosylase-treated FcγRIIIa ectodomain and identified several FcγRIIIa-specific Affimer proteins. We present two Affimer proteins and their structures derived from X-ray crystallography of their complexes with FcγRIIIa, allowing structures to be solved at atomic resolution. Molecular dynamics (MD) simulations based on the X-ray crystallographic models supported the molecular basis of Affimer protein's mode of action and selectivity for FcγRIIIa. One AffimerAffimer protein [Protein Data Bank (PDB) ID code 5ML9) bound close to the Fc-binding domain acting as a steric inhibitor, whereas the other (PDB ID code 5MN2) recognized an allosteric site and bound in the interdomain hinge region.

Our results demonstrate the feasibility of generating highly-specific inhibitors of protein-ligand interactions that bind unexplored sites and illustrate the utility of Affimer proteins in the study of protein function at both a molecular and cellular level.

Results

Identification and characterization of FcγRIIIa-specific Affimer proteins.

The extent of the challenge faced when developing specific agents against FcγRIIIa is illustrated by the structural alignment of FcγR crystal structures, demonstrating the high degree of target homology (**Fig. 1a)**. This is particularly true for FcγRIIIa and FcγRIIIb; only two amino acids are consistently different between FcγRIIIa and both common human neutrophil alloantigen types (NA1 and NA2, highlighted in red **Fig. 1b**) of FcγRIIIb, where there are a further four polymorphic amino acids in FcγRIIIb (highlighted in yellow in Fif. 1B): NA2 has one morel site for N-linked glycosylation than FcγRIIIa (Asn64) and differs in having serine at residue 18, whereas FcγRIIIa and FcγRIIIb-NA1 have arginine at this locus.

For phage display we used FcγRIIIa ectodomain bait that had been produced in HEK293T cells in the presence of kifunensine and treated with endoglycosidase F1 to facilitate crystallization and to allow valid comparisons between structural and biophysical data. A total of 72 randomly chosen Affimer proteins were tested for binding to FcγRIIIa using phage ELISA after three rounds of selection. Of these 52 gave positive results, and DNA sequencing revealed six unique clones. The most frequently recovered Affimer proteins were expressed as soluble proteins. AfG3 differed from AfF4 in terms of primary sequence, being derived from different libraries; AfF4 has an extra VR on an N-terminal extension (NTE) (**Fig. 1c**). We measured the FcγRIIIa-AfF4 and -AfG3 interactions by isothermal titration calorimetry (ITC), fitting a 1:1 binding model which gave estimated the K_ds to be 217nM and 2.6μM respectively (**Fig. 1d**). These ITC measurements may represent underestimates of Kd, as the N-values of 0.6 and 0.8 for AfF4 and AfG3, respectively, may indicate the presence of an inactive proportion of the analyte.

When amine coupled to carboxymethylated dextran sensor chips, the soluble ectodomain of FcγRIIIa interacted with both AfF4 and AfG3 with rapid association and dissociation rates (**Fig. S1a**) and 1:1 stoichiometry, allowing fitting to a Langmuir kinetic model, with calculated K_Ds 963 nM for AfF4 and 253 nM for AfG3. Since kinetic measurements at high analyte concentrations were around the detection limits of the instrument used, we calculated steady state affinity from the same interactions, estimating the K_Ds to be 1.03μM for AfF4 and 2.77μM for AfG3. In addition we performed surface plasmon resonance (SPR) assays on fully glycosylated and endoglycosidase F1-treated FcγRIIIa immobilised via a biotinylated C-terminal Avitag on streptavidin-coated chips. The orientated receptor displayed higher steady-state affinity for AfF4 and AfG3 at ~860 and ~680nM, respectively, with negligible difference conferred by glycosylation (**Fig S1b**).

Affimer proteins block IgG binding with a high degree of FcγR specificity.

Since primary cells expressing FcγRIIIa also express a number of other FcγRs, human embryonic kidney (HEK)293 cells stably expressing individual FcγRs were constructed to test the specificity of each AffimerAffimer protein. Each gene was fused to a C-terminal SNAP tag (26), except FcγRIIIb which is GPI-linked to the membrane. For FcγRIIIa allotypes each C-terminal SNAP domain fusion was co-expressed with the common γ-chain of FcεR to facilitate cell surface expression.

We then assessed blockade of heat-aggregated IgG1 (HAG) binding on stably transfected HEK293 cells. Both AfF4 and AfG3 significantly reduced (p=0.01) HAG binding to FcγRIIIa (158V) (**Fig. 2a** and **b**). Our cellular assays on FcγR specificity demonstrated that AfF4 and AfG3 had only a marginal nonsignificant effect on the binding of HAG to ectopically-expressed FcγRIIa and FcγRIIIb, confirming considerably weaker interactions between the Affimer proteins and these homologous FcγRs (**Fig. 2a**).

Importantly for therapeutic applications, AfF4 and AfG3 inhibited HAG binding to both the FcγRIIIa-158F and -158V allotypes**.** These Affimer proteins also displaced bound HAG from FcγRIIIa-158V; the allotype with a greater affinity for IgG1 complexes (**Fig. 2c**)**.**

To understand how the Affimer proteins blocked FcγRIIIa function and achieved such high specificity, we determined the crystal structures of AfF4 and AfG3 in complex with the FcγRIIIa ectodomain. The crystals belonged to space groups $P2_12_12_1$ (AfF4) and $P2_1$ (AfG3), both diffracting to a resolution of 2.35 Å and were refined to convergence (R_{work}/R_{free} of 21.9/27.2% and 20.6/24.6%, respectively)(**Table 1)**. All structures demonstrated that the core AffimerAffimer protein scaffold maintained its compact structure while the variable regions formed contacts with FcγRIIIa (rmsd < 0.5 Å in all cases). For clarity of referencing amino acid positions in FcγRs and Affimer proteins, FcγRIIIa and FcγRIIIb will be referred to as “γa-“ and “γb-“ whereas Affimer proteins will be referred to as ”AfG3-“ and ”AfF4-“, respectively. The two selected Affimer proteins bound to opposite faces of the FcγRIIIa ectodomain with AfF4 interfacing with the two FcγRIIIa-discriminating residues γa-Gly129 and γa-Tyr140, and AfG3 making contacts with FcγRIIIa extracellular domains 1 and 2.

The FcγRIIIa residues contributing to IgG binding, described in Ferrara *et al.*(27) are depicted in light green on the receptor surface in **Figs. 3a** and **4a**. Analysis of PDB ID code 3SGJ coordinates using PISA [European Molecular Biology Laboratory-European Bioinformatics Institute (EMBL-EBI)] estimated the total buried surface area of this

interaction interface to be ~950Å^2 and estimated a solvation free energy gain of -8.4 kcal/mol, with the formation of 10 hydrogen bonds.

AffimerAfF4-FcγRIIIa cocrystal structure reveals a steric mode of inhibition.

AfF4 residues in the two VRs, VR1 and VR2, interacted with γa-Ile106-His107 and γa-His119-Asp148. Several residues in the AfF4 NTE (His5 to Ala10) also interfaced with FcγRIIIa. Analysis with PISA (EMBL-EBI) estimated that the total buried surface area of the FcγRIIIa-AfF4 interaction to be ~940Å^2, and estimated a solvation free energy gain of -9.0 kcal/mol, with the formation of 12 direct hydrogen bonds. All hydrogen bond pairings are listed in **Table S1**.

The overlapping buried surface area between IgG Fc and AfF4 totalled about half of the individual interfaces, suggesting that AfF4 probably acts as a competitive inhibitor of IgG (**Fig. S2**).

The AfF4-FcγRIIIa crystal structure shows that the AfF4 binding region includes two amino acids which discriminate between FcγRIIIa and FcγRIIIb - γa-Gly129/γb-Asp129 and γa-Tyr140/γb-His140 **(Fig. 3a)**. To provide atomistic insight into the preference of AfF4 for FcγRIIIa, we used MD simulations to compare the interactions of AfF4 with both FcγRIIIa and FcγRIIIb, by mutating the AfF4-FcγRIIIa complex *in silico* to resemble AfF4-FcγRIIIb-NA2. Simulations were performed in triplicate for 200ns for each complex. Calculations of the rmsd (**Fig. S3**) showed that triplicates remained stable during the timescale of the simulations, and that 200ns was sufficient for the RMSD to converge to a stable value, which indicates that no significant global conformational changes took place.

Simulations were first subjected to atomic fluctuation analysis (**Fig. S4**), a measure of the average per-residue mobility throughout the simulations, which identified that VR2 of AfF4 was more mobile. Visual inspection of simulations around the AfF4 VR2-FcγRIIIa interface confirmed mobility of VR2 and that the aromatic ring of γa-Y132 orientates towards γa-Gly129 in FcγRIIIa simulations and away from γb-Asp129 in FcγRIIIb NA2 simulations (**Fig. 3b** and **c**). This is likely due to steric clash of the tyrosine ring with the γb-Asp129 side chain, causing the ring to move position. In MD simulations, the absence of a sidechain in γa-Gly129 allows the AfF4-Phe57 (VR1) sidechain to sit on top of γa-Gly129. AfF4-Phe57 in this position may also contribute to a hydrophobic pocket centred on AfF4 VR2 and γa-Tyr132. Conversely, the presence of a sidechain in γb-Asp129 leads to steric clash with the AfF4-Phe57 sidechain. AfF4-Phe57 is therefore more mobile in FcγRIIIb-containing simulations (**Fig 3b**), which may further weaken the AfF4 VR2-γa-Tyr132 binding pocket. In summary,

AfF4 inhibits IgG binding to FcγRIIIa by steric blocking of the IgG binding site and the specificity mechanism of AfF4 is likely due to the variation at position 129 in FcγRIIIa/b, which leads to steric clash with a number of important binding residues.

AffimerAfG3-FcγRIIIa cocrystal structures revealed allosteric mode of inhibition

As described above, crystals of FcγRIIIa-AfG3 belonged to space group $P2_1$ with four chains in the asymmetric unit (chain A and B: FcγRIIIa; chain C and D: AfG3) withchain A and D forming one FcγRIIIa-AfG3 complex and chain B and C the other. Because there are fewer crystallisation contacts than chain A, chain B, and in particular D2 of chain B, is highly flexible resulting in poor local quality of the electron density map and a high average B factor (**Table S2**). The overall rmsd per alpha carbon (Cα) between the AD and BC complexes is nonetheless only 0.62Å (217 aligned atoms), with the differences entirely distal to the binding interface. Thus, the FcγRIIIa-AfG3 complex formed by chain A and D was used for all following analyses and as the template for MD simulations.

Analysis of the FcγRIIIa-AfG3 cocrystal with PISA (EMBL-EBI) gave a total buried surface area in the interface of ~710 Å^2 (estimated solvation free energy gain of -7.5 kcal/mol). All hydrogen bond pairings are listed in **Table S3**. AfG3 bound to the inter-domain hinge region of FcγRIIIa and there was no overlap with the IgG binding site **(Fig. 4a)**. AfG3 residue Phe52 (VR1) sits in a hydrophobic pocket formed by the main chain of γa-Arg97 and the sidechains of γa-Gln83, Trp98, and in particular forms CH-π interactions with γa-Tyr17 while AfG3 Gly51 [O] forms an H-bond with γa-Val99 [N]. γa-Trp98 intercalates between VR1 and VR2, forming water-mediated interactions to AfG3-Phe52 [O] and to AfG3-Gln83 [O]. The residues in VR2 that form sidechain interactions with FcγRIIIa are Gln83–Asn86. AfG3-Trp84 stacks on top of AfG3-His85, which stacks on top of γa-His87. In addition, they interact with the sidechains of γa-Arg18, γa-Gln83, γa-Glu85, and γa-Thr167. Importantly, γa-Arg18 is a discriminating residue between FcγRIIIa/FcγRIIIb-NA1 and FcγRIIIb-NA2 (γa-Arg18/γb-Ser18) and is key in the binding of AfG3, even though it does *not* interact directly with AfG3. Most of the hydrophilic interactions are *via* bridging water molecules. For instance, Wat520 is coordinated by γa-Tyr17, γa-Glu85 and the [O] of AfG3-His85 such that it is forced into an uncommon, but not disallowed, torsion angle conformation of φ = 59.2° and ψ = -100.1°. This positions the sidechain so that it interacts again *via* a water molecule (Wat37) with the backbone of γa-Val86, and is able to form the π-π-stacking interaction mentioned above. The

discriminatory γa-Arg18 is held in place by an ion pair with γa-Glu85, and interacts with Wat1 and Wat3, that in turn interact with the VR2 loop.

Triplicate MD simulations (200ns) of FcγRIIIa and FcγRIIIa mutated *in silico* to resemble FcγRIIIb, in complex with AfG3 were performed. H-bond analysis of the simulations identified a number of intra-molecular H-bonds that form between γa-Arg18 and D2 residues of FcγRIIIa, which facilitate the narrowing of the D1-D2 interdomain angle. Specifically, γa-Arg18 [O] participated in an intramolecular H-bond with γa-Gln94 [Nε2], γa-Arg18 [H] with γa-Ala95 [O] and γa-Arg18 [NH1/NH2] with γa-Glu166 [OE1/OE2] **(Table S4)**. In the MD simulations, γa-Arg18 was observed interacting with AfG3-VR2 through an H-bond between the γa-Arg18 [NH1/NH2] atoms and AfG3-Asn86 [OD1]. Conversely, in FcγRIIIb, γa-Ser18 preferred participating in intra-molecular H-bonds with neighbouring residues from D1 of FcγRIIIb (γb-Glu21 and γb-Leu20). H-bonds between FcγRIIIa and Wat520 and Wat615, as seen in the crystal, and between AfG3 and Wat517 were also observed in the MD simulations.

Narrowing of the inter-domain angle likely allows γa-Trp99 to move closer to AfG3, leading to intercalation of γa-Trp99 between VR1 and VR2 and the formation of several intermolecular H-bonds and an additional intra-molecular H-bond (**Fig 4b, S5**). Conversely, as γb-Ser18 in FcγRIIIb forms only a single weak inter-domain contact, the inter-domain angle does not narrow and γb-Trp99 is unable to form these contacts.

Measurement of the D1-D2 inter-domain angles (described by alpha carbon [Cα] atoms in γa-Gln83, -Trp90 and -Asn169) in unbound FcγRIIIb (1FNL), IgG-FcγRIIIa (3SGJ), and AfG3-FcγRIIIa (5MN2) identified hinge angles of 46°, 53° and 41°, respectively **(Fig. 4c** and **d)**.

To analyse how this change in the angle may affect IgG binding, we superimposed the D2 domains (γa-Trp90-Gln174) derived from our x-ray structure 5MN2 on the FcγRIIIa structure bound to IgG (3SGJ). This shows that the overall shape of IgG-binding site is not disturbed and that only D2 is involved in binding. However, very subtle small conformational changes upon AfG3 binding prevent IgG binding. For example, the stacking interaction of AfG3-Trp84, AfG3-His85 and γa-His87 stabilises the BC loop (Ile88 – Trp90) in a conformation that prevents AfG3-Trp90 from moving, leading to a steric clash with Pro329 in chain B of IgG. In summary, simulations demonstrated that the presence of γa-Arg18 in FcγRIIIa-AfG3, but not γb-Ser18 in FcγRIIIb-AfG3, allows direct interaction of γa-Arg18 with AfG3 and leads to narrowing of the D1-D2 inter-domain angle through multiple γa-Arg18-mediated inter-domain contacts. This narrowing effectively forms the AfG3 binding interface by bringing VR1, VR2 and γa-Trp99 into close proximity.

Our proposed mechanism of IgG blocking is thus allosteric restraint of the interdomain angle that typically opens to accommodate IgG-binding (28).

Affimer proteins block downstream effector functions in FcγRIIIa-expressing monocytic cells

We sought to demonstrate that AfF4 and AfG3 could block clinically relevant FcγRIIIa effector functions using the THP-1 monocytic cell line. We characterized the cell line and determined that THP-1 cells were of the *FCGR3A*-158FF, *FCGR2A*-131HH and *FCGR2C*-STP/STP genotype, rendering them incapable of functional FcγRIIc expression. This allowed us to select suitable monoclonal antibodies for evaluation of FcγR expression under different experimental conditions using flow cytometry. Staining with CD32-3D3 (which recognizes FcγRIIa-131R, FcγRIIb and FcγRIIc but not FcγRIIa-131H) represents FcγRIIb expression in this cell line. Transcriptional analysis also confirmed that FCGR3B transcript variant 3 (RefSeq NM_001002274) and FCGR3A, but not FCGR3B, were transcribed thus confirming that the anti-CD16 (3G8) staining was a true reflection of FcγRIIIa expression.

Following phorbol myristate acetate (PMA)-differentiation, THP-1 cells demonstrated marked up-regulation of FcγRIIIa (CD16) and increased expression of FcγRIIb (CD32-3D3) along with decreased expression of FcγRIIa (CD32-IV.3) and, to a lesser extent, FcγRI (CD64), compared with resting cells (**Fig. 5a**). The marked increase in FcγRIIIa expression following culture with PMA allowed us to test the ability of the Affimer proteins to inhibit effector functions in the presence or absence of FcγRIIIa expression.

The contribution of FcγRIIIa to HAG-induced TNF production was determined in both resting and PMA-differentiated THP-1 by assessing the level of inhibition obtained with FcγRIII-specific $F(ab')_2$ fragments (**Fig. 5b**). Our results showed that FcγRIIIa blockade with $F(ab')_2$ fragments resulted in a 34.5% increase in cells showing no TNF production following differentiation with PMA and no demonstrable inhibition in TNF production in resting THP-1 cells that do not express appreciable amounts of FcγRIIIa (**Fig. 5b).** We then assessed the ability of AfF4 and AfG3 to inhibit HAG-mediated TNF production. Resting THP-1 and PMA-differentiated THP-1 cells were pre-treated with the Affimer proteins and assessed for their ability to produce TNF in response to HAG. Each AffimerAffimer protein demonstrated inhibition of TNF production in PMA-differentiated THP-1 at a level comparable to that observed with the FcγRIIIa-specific $F(ab')_2$ fragment. Resting THP-1 that do not express FcγRIIIa display less than 10% inhibition of HAG-induced TNF production, consistent with the levels seen following blockade with the FcγRIIIa-specific $F(ab')_2$ fragment.

We then compared the ability of Affimer proteins to inhibit phagocytosis of IgG-opsonized *Escherichia coli* in both resting and PMA-differentiated THP-1 cells and compared this with the level of inhibition observed following pre-treatment with FcγRIII-specific $F(ab')_2$. Inhibition of phagocytosis by each of the Affimer proteins was only observed in PMA-differentiated THP-1 where FcγRIIIa was expressed, and at a comparable level to cells treated with FcγRIII $F(ab')_2$, consistent with data on inhibition of TNF production (**Fig. 5c**).

Discussion

We describe the isolation of highly specific steric and allosteric inhibitors of FcγRIIIa using AffimerAffimer protein technology. These Affimer proteins specifically block IgG immune complex (HAG) binding to FcγRIIIa, but not the closely-related FcγRIIIb and FcγRIIa, and also inhibit downstream effector functions, such as TNF release and phagocytosis. Whilethere are some FcγR class-specific monoclonal antibodies that recognise epitopes in the IgG binding site, no commercially available antibody is specific for FcγRIIIa. This lack of specificity has been demonstrated *in vivo* when both monocyte and neutrophil cytopenias were observed in clinical trials of the CD16-3G8 monoclonal antibody that recognises both FcγRIIIa (expressed on NK cells and some peripheral blood monocytes) and FcγRIIIb (expressed on neutrophils) (29). Preservation of neutrophil function offers the potential to dampen down inflammatory processes orchestrated by macrophages whilst leaving host immunity to infections afforded by neutrophils intact.

We have identified an AffimerAffimer protein (AfF4) that binds within the IgG-binding site and acts as a highly-specific steric inhibitor of IgG binding to FcγRIIIa but not to FcγRIIa or FcγRIIIb, as shown by HAG binding assays using HEK293 cells expressing a single FcγR allotype. Elucidation of the structural basis for this specificity may facilitate engineering of CD16 therapeutic antibodies to achieve increased selectivity for FcγRIIIa over FcγRIIIb. Through X-ray crystallography and MD simulations, we have shown that AfF4 specificity for FcγRIIIa is likely focussed around the region containing the FcγRIIIa/b discriminating residue (γa-Gly129/γb-Asp129), showing that subtle differences in primary sequence can lead to local changes in topology which can have knock-on effects on molecular recognition.

An allosteric site in the hinge region of FcγRIIIa was recognised by AfG3, which holds the receptor ectodomain in a restricted conformation, preventing the opening of the structure associated with IgG Fc binding and in particular γa-Trp90. A major attraction of targeting allosteric sites is that they may be less evolutionarily conserved, and therefore allosteric inhibitors can potentially be more selective. Interestingly, AfG3, although binding to FcγRIIIa at a seemingly conserved region to FcγRIIIb, showed high cellular specificity to FcγRIIIa. Our proposed mechanism of AfG3 specificity is that the presence of γaArg18 can organise a large number of intramolecular H-bonds that, when AfG3 b inds, creat a tight FcγRIIIa-AfG3 interface that cannot occur with FcγRIIIb.

The molecular design of Affimer protein, which employs a stable scaffold for the constraint of mflexible regions of variable amino acid sequences, uses the same successful strategy for generating specific protein-protein interactions as antibodies. The high plasticity of the VRs combinaed with the chemical heterogeneity achievable through the wide variety of sequences generated by phage display ensure that sufficient biochemical space is explored and conformational space is sufficient to discover Affimer proteins capable of discriminating between highly homologous receptors. AffimerHowever, the delicate balance of interactions involved implies that rational design of future inhibitors based on structural information alone may not be adequate and that each AffimerAffimer protein identified as a binder should be considered unique. Indeed, this may be why loop grafting can result in affinity differences between different scaffolds, for example as observed in ref. 30.

The effect of each AffimerAffimer protein on clinically relevant FcγRIIIa effector functions was confirmed by the TNF production and phagocytosis assays. Although FcγRI, FcγRIIa and FcγRIIIa are expressed on the monocyte-like THP-1 cells, the inhibition of these downstream functions was correlated with the greatly increased FcγRIIIa expression in THP-1 cells differentiated with PMA. TNF release is a relevant *in vitro* model of receptor signalling since immune complex-activated macrophages have been shown to release large amounts of TNF in rheumatoid arthritis (31).

AffimerAffimer protein technology therefore, represents a promising methodological approach for the generation of highly stable, easily expressed antibody mimetic reagents with capabilities to modulate protein function and protein-protein interactions. X-ray structures and molecular dynamics simulations of AffimerAffimer protein/FcγRIIIa complexes provide a structural basis for understanding the potential mechanism of inhibition. Written informed consent was provided for the use of healthy human donor cDNA as cloning template and was approved by the Leeds(East) National Health Service Research Ethics Committee (Ref: 04/Q1206/107). .

Accession codes.

Coordinates and structure factors have been deposited in the Protein Data Bank under the accession codes 5ML9 and 5MN2.

Scripts and unsolvated trajectories to enable re-creation of the MD simulations are available through a DOI (https://doi.org/10.5518/258).

Figure Legends

Figure 1. The challenge of structural homology and the selection of specific protein based inhibitors of FcγRIIIa.

(**a**) Superimposed crystal structures of three FcγR ectodomains are shown as ribbon diagrams in complex with a space filling model of the Fc domain of IgG1. FcγRIIa is shown in yellow (PDB ID code 3RY6), FcγRIIIa in purple (PDB ID code 3AY4) and FcγRIIIb in green (PDB ID code 1T83). (**b**) Structural homology between FcγRIIIa and FcγRIIIb. The four amino acids in yellow differ between the FcγRIIIb NA1 and NA2 allotypes; two amino acids in red discriminate FcγRIIIa from FcγRIIIb and the location of the FcγRIIIa-158F/V allotype is green. The FcγRIIIb-NA2 allotype has an extra N-linked glycosylation site at Asn64. Extracellular domains 1 and 2 are depicted in aqua marine (D1 residues 1-89) and wheat (D2 residues 90-74), respectively. (**c**) The aligned amino acid sequences of AfF4 and AfG3 highlighting the positions of variable region 1 (VR1), variable region 2 (VR2) and the affinity tag (AT). Note that AfF4 has an additional N-terminal extension variable region (NTE). Residue numbering within the variable regions is indicated. (**d**) Isothermal titration calorimetry of the FcγRIIIa-AfF4 and -AfG3 interactions with isotherms and data fits. FcγRIIIa was at 10µM in the sample cell and Affimer proteins were injected in 2µl additions of 100µM.

Figure 2. Affimer proteins AfF4 and AfG3 specifically reduce immune complex binding to FcγRIIIa.

Heat-aggregated human IgG (HAG) binding assays utilized HEK293 cells stably expressing the full-length Fcγ receptors. Cells were treated with each AffimerAffimer protein before the addition of HAG followed by anti-human $F(ab')_2$ fragments labelled with PE; binding was measured by flow cytometry.

(**a**) Top row. Representative examples of the effect of AfF4 and AfG3 on immune complex (HAG) binding on cells expressing FcγRIIa; the unfilled distribution represents the untreated cells and the gray distribution represents binding to cells pre-treated with AffimerAffimer protein. The filled black region represents background binding of $F(ab')_2$ fragments to the cells. The middle row shows both the Affimer proteins reduce HAG binding to cells expressing FcγRIIIa alone, whereas the bottom row shows Affimer proteins had little effect on HAG binding to cells expressing FcγRIIIb.

(**b**) Histograms showing the reproducibility of AfF4 and AfG3 inhibition of HAG binding to FcγRs expressed stably on HEK293 cells. Values are normalized to AffimerAffimer protein-

untreated (HAG only) measurements. Error bars indicate standard deviation within three biological replicates.

(**c**) Top and middle. Representative experiments that demonstrate both Affimer proteins (AfF4 and AfG3) reduce binding of heat-aggregated IgG1 to both common allotypes of FcγRIIIa -158F and -158V (upper and middle panels). The open black histograms show the binding of HAG to cells expressing FcγRIIIa. The effect of preloading the receptors with Affimer proteins for one hour before adding HAG is shown as a solid grey histogram. The filled black histograms are controls without HAG. The lower panels show both Affimer proteins displaced HAG from the 158V allotype when added after HAG.

* $P<0.05$, *** $P<0.001$ (two-tailed Student's *t*-test).

Figure 3. Molecular dynamics simulation reveals molecular basis of interaction specificity of AfF4 for FcγRIIIa over FcγRIIIb. (**a**) Overview of AfF4 (orange) interaction with FcγRIIIa/b (domain 1 in aqua marine, domain 2 in wheat) showing FcγRIIIa/b discriminating residues in red and IgG contacts in light green. N-linked glycans with distinguishable electron density in the crystal structures are depicted as sticks. Zoom box for panel c also shown. (**b**) AfF4 variable region interface in FcγRIIIa and FcγRIIIb from molecular dynamics simulations. AfF4 VR1 and VR2 are depicted as ensembles of snapshots taken at 20ns intervals in representative simulations of the FcγRIIIa- and FcγRIIIb-AfF4 interactions. Interatomic distances between γa/b-Gly/Asp129 [CA] and γa/b-Tyr132 [HH] are illustrated as dashed lines and represented in dynamic measurements in (c). In FcγRIIIa the γa-Tyr132 sidechain orientates towards γa-Gly129, enabling AfF4 VR2 to form stable hydrophobic interactions involving γa-Tyr132 and AfF4-Phe57. In FcγRIIIb the γb-Asp129 sidechain clashes with γb-Tyr132 causing the ring to orientate away from γb-Asp129. γb-Asp129 also clashes with AfF4-Phe57 leading to disruption of the AfF4 VR2 hydrophobic interaction and higher mobility of VR2 and AfF4-Phe57 in FcγRIIIb. **(c)** Interatomic distance d averaged over triplicate MD simulations of FcγRIIIa- and FcγRIIIb-AfF4 interactions.

Figure 4. Molecular basis of AfG3 selectivity for FcγRIIIa. (**a**) Overview of binding position of AfG3 (orange cartoon) to FcγRIII (D1 aqua marine, D2 wheat, IgG contacts in light green, polymorphic residues in yellow, FcγRIIIa discriminatory residues in red). The zoom window for panel **b** is indicated by the black box. (**b**) Molecular dynamics simulation pose of the interaction of AfG3 with FcγRIIIa (purple sticks) and FcγRIIIb (green sticks). γa-Trp98 intercalates between AfG3 VR1 and VR2 resulting in several stable intermolecular H-bonds, whereas in FcγRIIIb these contacts did not form in the MD simulations. (**c**) Cartoon

representation of FcγRIIIa (aqua marine and wheat) interacting with IgG Fc (salmon). The interdomain angle Θ is described by lines connecting the [CA] of γa-Trp90 at the top of the hinge, and the [CA] of Asn169 in D2 and the [CA] of Gln83 in D1. Mode vectors describing the allosteric change from the IgG-bound state to the AfG3-bound state are represented as blue arrows. Mode vectors shorter than 3Å not shown. (**d**) Schematic representation of the allosteric change induced by AfG3. Unbound FcγRIII (PDB 1FNL) describes a D1-D2 interdomain angle Θ of 46° which opens to 53° on interaction with IgG Fc. FcγRIIIa interaction with AfG3 narrows the D1-D2 angle by 12° to 41° and we hypothesize that this allosteric shift causes sufficient deformation of the IgG Fc binding site to induce IgG Fc displacement.

Figure 5. Affimer proteins are effective inhibitors of FcγRIIIa – dependent functions. (**a**) FACs profiles for resting, monocytic THP-1 cells (left side) and PMA-differentiated, macrophage-like THP-1 cells (right side). In each case, the specific antibody staining is shown as an unfilled distribution whereas the isotype control staining is shown as a filled distribution. The high affinity FcγRIa (CD64) is reduced in differentiated THP-1 cells, along with the activatory FcγRIIa (CD32-IV.3). The inhibitory FcγRIIb is upregulated in differentiated cells along with FcγRIIIa. **(b)** Affimer proteins were more effective in blocking HAG-induced TNF release in differentiated cells (upper right panel) than undifferentiated (upper left panel), confirming their specificity for FcγRIIIa. This is represented as an increase in the percentage of TNF negative cells. The upper panels also show blocking $F(ab')_2$ fragments against FcγRIIIa inhibit TNF production only in differentiated THP-1 cells. $F(ab')_2$ fragments against FcγRIII (CD16) are far more effective in differentiated cells (upper panel, right) reflecting the differences in FcγRIIIa expression, shown in **a**. $F(ab')_2$ fragments from preimmune serum had no effect on TNF production. The lower panels show both Affimer proteins are as effective in reducing phagocytosis of IgG opsonised *E Coli* as $F(ab')_2$ fragments in differentiated THP-1 cells.

Acknowledgements

We acknowledge the University of Leeds and Leeds Teaching Hospitals NHS Trust funding for the Leeds Biomedical Health Research Centre BioScreening Technology Group (BSTG). We thank Mr. Thomas Taylor of the Leeds Biomedical Healtch Research |Centre BioScreening Technology Group (BSTG) for excellent technical support. ITC was performed in the Astbury Biomolecular Interactions Facility, supported by the Wellcome Trust, 094232/Z/10/Z. The work undertaken on beamline I24 at Diamond Light Source was under proposal NT5969. The Medical Research Council (grant MR/K018779/1) supported the

Oxford Protein Production Facility was supported by Medical Research Council Grant MR/K018779/1. The research was also supported by Arthritis Research UK Grant 19764, the National Institute for Health Research (NIHR) Leeds Biomedical Research Centre, the Ann Wilks Memorial Fund, and Biotechnology and Biological Research Council Grant BB/M021610/1. This work was further supported by a grant byMarie Skłodowska-Curie Actions in Horizon 2020 (to M.T.). The Leeds Biomedical Health Research Centre BSTG received funding from the University of Leeds and Leeds Teaching Hospitals NHS Trust. The views expressed are those of the author(s) and not necessarily those of the NHS, the NIHR or the Department of Health.

Contributions

J.I.R., E.W.B., D.C.T., R.J.F., R.J.O., S.A.H., M.J.M., and A.W.M. designed research; J.I.R., E.W.B., M.P.W., S.J.W., J.E.N., and C.T. performed research; D.C.T., C.T., C.W.G.F., and S.A.H. contributed new reagents/analytic tools; J.I.R., E.W.B., R.L.O., M.T., M.P.W., S.J.W., J.E.N., C.W.G.F., S.A.H., and A.G. analyzed data; and J.I.R., E.W.B., M.T., D.C.T., M.P.W., S.A.H., A.G., M.J.M., and A.W.M. wrote the paper.

Conflict of interest statement: The University of Leeds has filed a patent application on AffimerAffimer protein (referred to here as Affimer protein) that is licensed to Avacta Life Sciences Ltd.

References

1. Milroy, L.-G., Grossmann, T.N., Hennig, S., Brunsveld, L. & Ottmann, C. Modulators of Protein–Protein Interactions. Chemical Reviews 114, 4695-4748 (2014).

2. Higueruelo, A.P., Jubb, H. & Blundell, T.L. Protein–protein interactions as druggable targets: recent technological advances. Current Opinion in Pharmacology 13, 791-796 (2013).

3. Jubb, H., Higueruelo, A.P., Winter, A. & Blundell, T.L. Structural biology and drug discovery for protein–protein interactions. Trends in Pharmacological Sciences 33, 241-248 (2012).

4. Reichert, J.M., Rosensweig, C.J., Faden, L.B. & Dewitz, M.C. Monoclonal antibody successes in the clinic. Nat Biotechnol 23, 1073-1078 (2005).

5. Vlasak, J. & Ionescu, R. Heterogeneity of Monoclonal Antibodies Revealed by Charge-Sensitive Methods. Current Pharmaceutical Biotechnology 9, 468-481 (2008).

6. Tiede, C. et al. AffimerAffimer protein: a stable and versatile peptide display scaffold for molecular recognition patterns. Protein Engineering Design and Selection 27, 145-155 (2014).

7. Sharma, R. et al. Label-free electrochemical impedance biosensor to detect human interleukin-8 in serum with sub-pg/ml sensitivity. Biosensors and Bioelectronics 80, 607-613 (2016).

8. Rawlings, A.E. et al. Phage display selected magnetite interacting Affimer proteins for shape controlled nanoparticle synthesis. Chemical Science 6, 5586-5594 (2015).

9. Kyle, H.F. et al. Exploration of the HIF-1[small alpha]/p300 interface using peptide and AffimerAffimer protein phage display technologies. Molecular BioSystems 11, 2738-2749 (2015).

10. Modell, A.E., Blosser, S.L. & Arora, P.S. Systematic Targeting of Protein-Protein Interactions. Trends in Pharmacological Sciences 37, 702-713.

11. Nimmerjahn, F. & Ravetch, J.V. Fcg receptors as regulators of immune responses. Nat Rev Immunol 8, 34-47 (2008).

12. Hogarth, P.M. & Pietersz, G.A. Fc receptor-targeted therapies for the treatment of inflammation, cancer and beyond. Nat Rev Drug Discov 11, 311-331 (2012).

13. Morgan, A.W. et al. Association of FCGR2A and FCGR2A-FCGR3A haplotypes with susceptibility to giant cell arteritis. Arthritis Research & Therapy 8, R109 (2006).

14. Robinson, J.I. et al. Association of FCGR3B, but not FCGR3A copy number, with susceptibility to rheumatoid arthritis: functional correlation with reduced neutrophil Fc gamma RIIIb expression. Immunology 131, 123 (2010).

15. Willcocks, L.C. et al. Copy number of FCGR3B, which is associated with systemic lupus erythematosus, correlates with protein expression and immune complex uptake. Journal of Experimental Medicine 205, 1573-1582 (2008).

16. Cooper, D.L. et al. FcgRIIIa expression on monocytes in rheumatoid arthritis: role in immune-complex stimulated TNF production and non-response to methotrexate therapy. PLoS ONE 7, e28918 (2012).

17. Ji, H. et al. Arthritis critically dependent on innate immune system players. Immunity 16, 157-168 (2002).

18. Kleinau, S., Martinsson, P. & Heyman, B. Induction and suppression of collagen-induced arthritis is dependent on distinct Fcg receptors. J Exp Med 191, 1611-1616 (2000).

19. Qiu, W.Q., de Bruin, D., Brownstein, B.H., Pearse, R. & Ravetch, J.V. Organisation of the human and mouse low-affinity FcgR genes: duplication and recombination. Science 248, 732-735 (1990).

20. Machado, L.R. et al. Evolutionary history of copy-number-variable locus for the low-affinity Fc receptor: mutation rate, autoimmune disease, and the legacy of helminth infection. American Journal of Human Genetics 90, 973-985 (2012).

21. Clarkson, S.B. et al. Treatment of refractory immune thrombocytopenic purpura with an anti-Fc gamma-receptor antibody. New England Journal of Medicine 314, 1236-1239 (1986).

22. Bosques, C.J. & Manning, A.M. Fc-gamma receptors: attractive targets for autoimmune drug discovery searching for intelligent therapeutic designs. Autoimmunity Reviews 15, 1081-1088 (2016).

23. Weinblatt, M.E. et al. Effects of Fostamatinib (R788), an Oral Spleen Tyrosine Kinase Inhibitor, on Health-related Quality of Life in Patients with Active Rheumatoid Arthritis: Analyses of Patient-reported Outcomes from a Randomized, Double-blind, Placebo-controlled Trial. Journal Of Rheumatology 40, 369-378 (2013).

24. Friedburg, J.W. et al. Inhibition of Syk with fostamatinib disodium has significant clinical activity in non-Hodgkin lymphoma and chronic lymphocytic leukemia. Blood 115, 2578-2585 (2010).

25. MacFarlane, L.A. & Todd, D.J. Kinase inhibitors: The next generation of therapies in the treatment of rheumatoid arthritis. International Journal of Rheumatic Diseases 17, 359-368 (2014).

26. Keppler, A. et al. A general method for the covalent labeling of fusion proteins with small molecules in vivo. Nat Biotech 21, 86-89 (2003).

27. Ferrara, C. et al. Unique carbohydrate-carbohydrate interactions are required for high affinity binding between FcgRIII and antibodies lacking core fucose. Proceedings of the National Academy of Sciences 108, 12669-12674 (2011).

28. Woof, J.M. & Burton, D.R. Human antibody-Fc receptor interactions illuminated by crystal structures. Nat Rev Immunol 4, 89-99 (2004).

29. Nakar, C.T. & Bussel, J.B. 3G8 and GMA161, Anti FcγRIII Inhibitory Monoclonal Antibodies in the Treatment of Chronic Refractory ITP. (Summary of 2 Pilot Studies). Blood 114, 2404-2404 (2009).

30. Vita, C. et al. Novel miniproteins engineered by the transfer of active sites to small natural scaffolds. Biopolymers 47, 93-100 (1998).

31. Cassatella, M.A. et al. Soluble TNF-like cytokine (TL1A) production by immune complexes stimulated monocytes in rheumatoid arthritis.[Erratum appears in J Immunol. 2007 Jul 15;179(2):1390 Note: da Silva, Gabriela Pereira [corrected to Pereira-da-Silva, Gabriela]]. Journal of Immunology 178, 7325-7333 (2007).

32. Berrow, N.S., Alderton, D. & Owens, R.J. The Precise Engineering of Expression Vectors Using High-Throughput In-Fusiontrade mark PCR Cloning. Methods Mol Biol 498, 75-90 (2009).

33. Bird, L.E. High throughput construction and small scale expression screening of multi-tag vectors in Escherichia coli. Methods 55, 29-37 (2011).

34. Nettleship, J.E., Rahman-Huq, N. & Owens, R.J. The production of glycoproteins by transient expression in mammalian cells. Methods Mol Biol 498, 245-263 (2009).

35. Chomczynski, P. & Sacchi, N. Single-step method of RNA isolation by acid guanidinium thiocyanate -phenol-chloroform extraction. Analytical Biochemistry 162, 156-159 (1987).

36. Tiede C, et al. (2017) Affimer proteins are versatile and renewable affinity reagents. Elife 6:e24903.

37. Warmerdam, P.A.M. et al. Interaction of a human FcgRIIb1 (CD32) isoform with murine and human IgG subclasses. Int Immunol 5, 239-247 (1993).

38. Daeron, M. et al. The same tyrosine-based inhibition motif, in the intracytoplasmic domain of Fc gamma RIIB, regulates negatively BCR-, TCR-, and FcR-dependent cell activation. Immunity 3, 635-646 (1995).

39. Morgan, A.W. et al. Analysis of Fcγ Receptor haplotypes in rheumatoid arthritis. FCGR3A remains a major susceptibility gene at this locus with an additional contribution from FCGR3B. Arthritis Research & Therapy 8, R5 (2006).

40. Metes, D. et al. Expression of functional CD32 molecules on human NK cells is determined by an allelic polymorphism of the FcgRIIC gene. Blood 91, 2369-2380 (1998).

41. Walter, T.S. et al. A procedure for setting up high-throughput nanolitre crystallization experiments. Crystallization workflow for initial screening, automated storage, imaging and optimization. Acta Crystallogr D Biol Crystallogr. 61, 651-657 (2005).

42. Kabsch, W. XDS. Acta Crystallographica Section D 66, 125-132 (2010).

43. Evans, P.R. & Murshudov, G.N. How good are my data and what is the resolution? Acta Crystallographica Section D 69, 1204-1214 (2013).

44. McCoy, A.J. et al. Phaser crystallographic software. Journal of Applied Crystallography 40, 658-674 (2007).

45. Afonine, P.V. et al. Towards automated crystallographic structure refinement with phenix.refine. Acta Crystallographica Section D 68, 352-367 (2012).

46. Emsley, P., Lohkamp, B., Scott, W.G. & Cowtan, K. Features and development of Coot. Acta Crystallographica Section D 66, 486-501 (2010).

47. Chen VB, et al. (2010) MolProbity: All-atom structure validation for macromolecular crystallography. Acta Crystallogr D Biol Crystallogr 66:12–21.48. Tina, K.G., Bhadra, R. & Srinivasan, N. PIC: Protein Interactions Calculator. Nucleic Acids Res 35, W473-W476 (2007).

49. Case, D.A. et al. AMBER 14, University of California, San Francisco. (2014).

50. Maier, J.A. et al. ff14SB: Improving the Accuracy of Protein Side Chain and Backbone Parameters from ff99SB. Journal of Chemical Theory and Computation 11, 3696-3713 (2015).

51. Kirschner, K. N. et al. GLYCAM06: A generalizable biomolecular force field. Carbohydrates. J. Comput. Chem., 29, 622–655. 2008,

52. Prokop, M., Adam, J., Kříž, Z., Wimmerová, M. & Koča, J. TRITON: a graphical tool for ligand-binding protein engineering. Bioinformatics 24, 1955-1956 (2008).

53. Humphrey, W., Dalke, A. & Schulten, K. VMD: visual molecular dynamics. J Mol Graph 14, 33-8, 27-8 (1996).

54. Schrödinger, LLC (2010) The PyMOL Molecular Graphics System, Version 1.2r3pre. (Schrödinger, LLC, New York), Version 1.2r3pre.

Supplementary Information

Methods

All reagents were purchased from Sigma–Aldrich (Dorset, UK) unless stated otherwise.

FcγR Cloning Strategy

FcγR ectodomains (FcγRIIIa 158F, FcγRIIa 131H) were amplified by PCR (see **Table S4** for primer sequences) and cloned into pOPINTTG (OPPF) using the InFusion system (Clontech Laboratories Inc.)(32, 33).

Alternative allotypes (FcγRIIIa-158V, FcγRIIa-131R) were produced using QuikChange Lightning (Agilent Technologies) following the Manufacturer's protocol. Constructs were tested for expression of secreted protein on a 1ml scale using transient transfection of HEK293T cells (ATCC) and analysis of the supernatant by anti-His Western blot (Roche), as previously described(34).

Full-length coding sequences encoding FcγRIIa (131R) and FcγRIIIb (NA2) were amplified from cDNA from peripheral blood mononuclear cells from genotyped donors. Full-length coding sequences encoding FcγRIIIa (158F) were amplified from THP-1 cells using cDNA prepared by reverse transcriptase PCR (RT-PCR) of total RNA extracted using acid phenol/ guanidinium hydrochloride and isopropanol precipitation(35) with Superscript II reverse transcriptase (Invitrogen) and oligo dT primers (see **Table S4** for details of primers used). These sequences were cloned into a plasmid encoding the enzymatic SNAP tag (New England Biolabs) derived from pFB HYG (a gift from Dr. J.E. Burns). The plasmids were used to transfect Phoenix A packaging cells (Nolan labso that replication-defective virus particles were produced in the supernatant. These supernatants were filtered and used to infect HEK293 cells (in the case of FcγRIIIa–expressing cells, virus particles were used to infect cells which had already been infected with a neo resistance vector for stable expression of the common γ-chain of FcεRI gene (*FCER1G*, NM_004106.1). This double transfection was carried out to allow cell surface expression of FcγRIIIa which is dependent on the common γ-chain of FcεRI). Primer sequences for the common γ-chain of FcεRI are shown in **Table S4.** After 10 days of antibiotic selection, the cells were tested for surface expression using FITC-labelled anti-CD16 mouse monoclonal DJ130c (Dako) which recognises an epitope in the first extracellular domain. This antibody was also used to show expression of FcγRIIIb. Expression of ectopically-expressed FcγRIIa was tested using mouse monoclonal AT10 (CD3204, Caltag-Medsystems).

Protein production and purification

Proteins were secreted from HEK293T adherent cells in roller bottles. Purification was by immobilized metal affinity chromatography followed by gel filtration chromatography using a Superdex 200 column. Purified fractions were pooled and concentrated. FcγRIIIa-158F and 158V produced 1-2mg per L of culture. To produce protein for co-crystallization, the cells were grown in the presence of the glycosylation inhibitor kifunensine (Toronto Research Chemicals) resulting in ectodomains with glycans of the form $Man_9GlcNAc_2$. To give protein with glycans of the form $GlcNAc_1$, the purified protein was treated with Endoglycosidase F1 overnight at 4°C and then further purified by gel filtration chromatography to remove the glycosidase and trimmed glycans from the sample. To assess the effect of FcγRIIIa glycosylation on the Affimer interaction in SPR, the proteins were produced as above, but without kifunensine. A portion of the glycosylated protein was treated with Endoglycosidase F1 as described.

For some experiments, FcγRIIIa ectodomains were biotinylated using EZ-link NHS-SS-biotin (Thermo Fisher Scientific), according to the manufacturer's instructions. Biotinylation was confirmed using streptavidin-conjugated to horseradish peroxidase (HRP) to detect the biotin on FcγRIIIa absorbed onto Nunc Immuno Microwell™ MaxiSorp™ 96-well plates (Thermo Fisher Scientific).

In vitro selection of FcγRIIIa-specific Affimers

a. *Phage display*

We used the libraries described in refs. 6 and 36. We used purified, endoglycosidase F1–treated and biotinylated FcγRIIIa ectodomain (158V) protein as the screening target in phage display. In brief, 5µl of the phagemid library (10^{12} colony forming units), was pre-panned three times in high binding capacity streptavidin coated wells (Thermo Fisher Scientific) for a total of 1hr. The phage were then incubated with biotinylated FcγRIIIa for 2.5hrs. Panning wells were washed 10 times and eluted with 100µl of 50 mM glycine-HCl (pH 2.2) for 10mins, neutralised with 1M Tris-HCl (pH 9.1), and further eluted with 100µl of triethylamine 100mM for 6mins and neutralised with 50µl of 1M Tris-HCl (pH 7). Eluted phage were incubated with exponentially growing ER2738 cells (OD_{600} = 0.6) for 1hr at 37°C and plated onto Lysogeny Broth (LB) agar plates. The following day phage were propagated overnight and used in a second panning round displaying FcγRIIIa on streptavidin magnetic beads. Phage/beads were incubated with mixing then washed 5 times using a KingFisher robotic

platform (ThermoFisher Scientific), then eluted and amplified as above. The final pan was performed using neutravidin high binding capacity plates (ThermoFisher, Scientific), as described above, but the phage were eluted on a vibrating platform for 20min with 100µl 100mM dithiothreitol to reduce the disulphide bond of the EZ-link NHS-SS-biotin, prior to infection of ER2738 cells. Phage were recovered from wells containing FcγRIIIa and control wells to determine the level of amplification in target wells.

b. Binding specificity by ELISA

Phage ELISA was performed as previously described(6). Streptavidin coated plates (Thermo Fisher Scientific) were blocked, labelled with 0.4 nM of biotinylated FcγRIIIa for 1hr, and 45µl of growth medium containing phage propagated from individual clones was added to wells containing biotinylated FcγRIIIa or a well containing only the biotinylated linker and incubated for 1hr. After washing 3 times in 300µl phosphate buffered saline with Tween20 (PBST), and a 1:1000 dilution of HRP-conjugated anti-phage antibody (Seramun Diagnostica GmBH) in 100µl PBST was added for 1hr. Wells were washed 10 times in 300µl PBST and Affimer-mediated phage binding were visualised with 100µl 3,3′,5,5′-Tetramethylbenzidine (TMB) liquid substrate (Seramun Diagnostica GmBH) and absorbance measured at 560 nm. Positive binders were submitted for DNA sequence analysis (Beckman Coulter Genomics).

c. Recloning and modifications

The coding sequences of selected Affimer proteins were PCR amplified, restriction digested with *Nhe*I and *Pst*I and cloned into pET11a containing the Affimer proteins scaffold coding region. For biotin labelling Affimer proteins were cloned into a pET11a-scaffold construct encoding a C-terminal cysteine. Individual clones were sequenced to confirm the presence of the correct insert. Plasmids were transformed into BL21 (DE3) cells and cultures grown in 400ml of LB medium to an OD_{600} of 0.6 at 37°C, before addition of isopropyl β-D-1-thiogalactopyranoside to 1mM. After a further 6hr, cells were harvested, resuspended in 25ml of 1x Bugbuster (Novagen,) with benzonase, mixed for 20min, then heated to 50°C for 20min. The cleared supernatant was mixed with 500µl Ni-NTA resin (Expedeon) for 1hr, washed 3 times in 30ml wash buffer (50mM phosphate buffered saline (PBS), 500mM NaCl, 20mM imidazole, pH 7.4) and eluted in 1ml of elution buffer (50mM PBS, 500mM NaCl, 300mM imidazole, pH 7.4).

d. *Confirmation of FcγRIIIa binding*

Freshly purified Affimer proteins were used in surface plasmon resonance (SPR) assays to confirm binding to both common FcγRIIIa allotypes (158F and V). SPR was carried out on a

BIAcore T200 biosensor (GE Healthcare). Soluble FcγRIIIa ectodomains of the 158V allotype were immobilised (100RU) in 10mM acetate pH5.0 on a CM5 sensor chip (GE Healthcare) using amine coupling, as directed by the manufacturer. Affimer proteins were used as analytes in single cycle kinetics with 2min injections of increasing concentrations from 123nM through to 10µM at a flow rate of 30µl/min in HBS-EP+ running buffer. The FcγRIIIa surface was regenerated between cycles using a 60s injection of 10mM glycine pH2.0 at 30µl/min.

A blank amine coupled flow cell was used as reference and zero concentration controls were used in double-referencing. All analysis was carried out using the BIAcore T200 Evaluation Software v1.0. Langmuir 1:1 kinetic models were fitted to reference-subtracted sensorgrams and steady state affinity models were fitted.

For isothermal titration calorimetry (ITC), protein samples were dialysed against PBS overnight at 4°C and this buffer was used for control titrations. ITC was performed using an iTC200 instrument (Microcal, Malvern Instruments) at 25°C. An initial injection of 0.5µl over 1 second was followed by 19 injections of 2µl over 4 seconds each, with 2 minute spacing, while stirring at 750rpm and with a reference power of 5µCal/sec. The sample cell contained 10µM FcγRIIIa-158V and Affimer protein was injected at a concentration of 100µM. Results were analysed using Origin software after subtraction of a control titration of Affimer protein into buffer.

Cell-based IgG binding assays

Constructs encoding FcγRIIa (27Q 131H), FcγRIIIa (158F and V) and FcγRIIIb-NA2 were stably transfected into HEK293 cells and used to investigate FcγRIIIa-specific inhibition of IgG1 HAG binding. Cells were harvested with trypsin and EDTA then resuspended at 250 cells/µl in Dulbecco's Modified Eagle's medium (Invitrogen, Paisley, UK) containing 10% fetal calf serum (FCS). Each selected Affimer protein was added at 50µg/ml incubated at room temperature for 1hr. The cells were cooled on ice and incubated with 100µg/ml heat-aggregated gamma globulin (HAG) (The Binding Site) for a further 2 hours. The cells were incubated on ice for 1hr with 100x diluted goat anti-human κ light chain $F(ab')_2$ fragments labelled with phytoerythrin (PE) (AbD Serotec, BioRad). Cells were washed in ice-cold FACS buffer (PBS with 2%FCS and 2mM EDTA) then fixed in 2% formaldehyde to prevent loss or phagocytosis of complexes. Binding of HAG to the FcγR-expressing cells was assessed using a Guava EasyCyte Flow Cytometer (Millipore) using empty vector–transfected cells as controls.

The median fluorescence Intensity (MFI) was determined for each tube and averages of triplicate values were determined for each cell line. Statistical significance was calculated by using two-tailed Student's *t*-tests for inhibition of HAG binding and an assumption of unequal variance.

Blockade of effector functions in the THP-1 macrophage cell line

a. Characterization of the FcγR expression on THP-1 cells under different culture conditions.

In order to select suitable monoclonal antibodies for these studies we undertook some genetic and transcriptional analysis of the THP-1 cell line. The extracellular domains of the CD32 receptors (FcγRIIa, FcγRIIb and FcγRIIc) are almost identical and consequently not all CD32 mAbs are able to fully distinguish between the FcγRII subtypes. CD32-IV3 (Stem cell Technologies, Marseille, France) has been reported to recognise only FcγRIIa (36, 37). Whereas, CD32 3D3 (BD Pharmingen, Oxford, UK) recognises FcγRIIa-131R, FcγRIIb and FcγRIIc. The THP-1 cell line was therefore genotyped for *FCGR2A*-131H/R by direct sequencing of genomic DNA, using published assays (38). The *FCGR2C* STP/ORF variant and transcription of specific FcγRIIb/c isoforms were determined as described in (39).

Human monocytic THP-1 cells (European Collection of Cell Cultures) were grown in RPMI 1640 containing 10% FCS, 2mM L-glutamine at 37°C in 5% CO_2. The level of FcγR cell surface expression was initially determined in resting and PMA-differentiated THP-1 cells. Briefly, THP-1 cells were seeded at a density of 2 x10^5 cells/ml and incubated with media alone or 50ng/ml PMA for 18hr at 37°C. The medium containing PMA was removed and the cells rested for 48hr in the presence of medium alone.

The level of expression of cell surface markers (FcγRIII: CD16-3G8, Caltag-Medsystems, CD32-IV.3, Stem cell Technologies) and CD32-3D3, BD Pharmingen, CD64-10.1, Beckman Coulter Immunotech) and the percentage of cells positive for these markers were evaluated in differentiated THP-1 cells incubated for an additional 24hr in the presence of medium alone or following stimulation with 250ng/ml lipopolysaccharide (LPS). Cells harvested using trypsin and EDTA were washed in PBS-bovine specific albumin (BSA), stained with directly conjugated antibodies (diluted 250x, 30min, 4°C, in dark), washed with PBS-BSA, resuspended in PBS-BSA and analysed by flow cytometry (Becton Dickinson LSRII).

a. TNF production

TNF production was assessed in differentiated THP-1 cells (2 x 10^5 cells in 500µl) that were incubated for 1hr at 37°C in medium alone (negative control), or with 250ng/ml LPS (positive

control) or with 100µg/ml HAG prior to addition of 10µg/ml brefeldin A (intracellular protein transport inhibitor) and further incubation for 3hr (37°C, 5% CO_2). Blocking antibodies were obtained from Ancell Corporation. The antibody clones were 3G8 for CD16 (a known blocking Ab), 7.3 for CD32 and 10.1 for CD64. Cells were washed in PBS- 2%BSA, fixed in 2% paraformaldehyde for 30min, washed again and then permeabilized using 0.3% saponin in PBS-BSA (15min, room temp.). Anti-TNF-phycoerythrin (PE) or IgG1-PE (Serotec, Oxford, UK) diluted 1: 500 in PBS-BSA + 0.1% saponin were added for 30min (room temp. in dark), washed and resuspended in PBS-BSA for immediate analysis by flow cytometry (Becton Dickinson LSRII).

b. *Phagocytosis of IgG-opsonised* E. coli

Phagocytosis was assessed by incubation of differentiated THP-1 cells (2 x 10^5 cells/ml) with either 10 µg/ml *E. coli* (Invitrogen) alone or *E. coli* pre-opsonised with 5% human AB serum (complement inactivated: 56°C, 30min), followed by washing (1600 x g, 15min) to remove excess serum) for 1hr at 37°C, or in cells pre-cooled to 4°C (negative control). Cells were washed in PBS-BSA, stained with 0.4% trypan blue to quench extracellular fluorescence, washed three times with PBS-BSA and resuspended in PBS-BSA and analysed by cytometry (Becton Dickinson, LSRII).

Crystallisation and Structure Solution

Endoglycosidase F1-treated FcγRIIIa crystals 20-30 µm in size were grown in 200nl drops (100nl FcγRIIIa ectodomain + 100nl precipitant) in 96-well plates using non-contact dispensing robotics (Microsys Cartesian). Crystallization trials used the method of Walter *et al.*(40) at 8.9 mg/ml for 158F and at 11.4 mg/ml for 158V. Co-crystallization of FcγRIIIa with Affimers was performed by mixing the proteins in a 1:1 molar ratio and incubating at room temperature for 30mins before setting up crystallization trials. Conditions are shown in **Table S3**.

Crystals were detected in a number of conditions with data being collected from condition 41 or 43 of the Hampton PEG / Ion screen (20% (w/v) polyethylene glycol 3350, 0.200 M potassium di-hydrogen phosphate and 20% (w/v) polyethylene glycol 3350, 0.200 M ammonium pPhosphate monobasic) or optimizations around these conditions(40).

For diffraction data collection, crystals were loop mounted and cryo-cooled in liquid nitrogen. Data were collected at Beamline I24, Diamond Light Source, with the X-ray beam defocused to 20×20 μm^2 from multiple positions on each crystal. All diffraction data were integrated using XDS(41) and scaled using AIMLESS(42). Phases were obtained via molecular

replacement using PHASER(43). A subsection of a complex of an Affimer protein bound to a soluble protein was used as a search model. Refinement was carried out using PHENIX(44). Ligands and sugar modifications were built manually into *Fo- Fc* maps using COOT(45). In the case for AdG3 additional noncrystallographic symmetry torsion restraints were applied during refinement. The quality of the protein structure was assessed using MOLPROBITY. Data collection and refinement statistics are given in Table 1.

The residues involved in Affimer protein binding to FcγRIIIa were identified based on the Protein Interaction Calculator(46) and visual inspection.

Molecular dynamics simulations.

Molecular dynamics (MD) simulations were prepared with the AmberTools 14 suite of programs and performed with AMBER14 (47), ff14SB47 (48) and GLYCAM_06j-1 (49). Simulations used 128 processors of the MARC1 supercomputer available at Leeds. To simulate Affimer protein-FcγR interactions in water, models were first generated of each Affimer protein in complex with either FcγRIIIa (-158F allotype for AdG3 and -158V allotype for AdF4) or FcγRIIIb-NA2. The FcγRIIIb-containing complex was generated by mutation of the FcγRIIIa-Affimer protein crystal structures to resemble the FcγRIIIb-NA2 through the use of TRITON/MODELLER (50).

After mutagenesis, the xleap program of AmberTools 14 was used to add hydrogen atoms, form disulphide bridges and add β1,4 linked D-N-acetyl glucosamine (GlcNAc) residues at glycosylation sites in FcγRIIIa/FcγRIIIb. Complexes were then placed in a TIP3P water box with a 10.0-Å cut-off, and the system was neutralized with Na+ ions. The system was equilibrated through an initial energy minimization, which was followed by 80ps of restrained molecular dynamics during which the system was heated to 300K with gradual releasing of restraints. An unrestrained MD simulation of 200ns was then performed. For each complex, simulations were repeated in triplicate.

Calculations of the Root Mean Square Deviation (RMSD) showed that all simulations remained stable, and that 200ns was sufficient for the RMSD to converge to a stable value, which indicates that no significant global conformational changes are taking place over MD timescales.

Desolvated trajectories were analysed with the cpptraj module of AMBER14, which was used to calculate inter- and intra-molecular H-bonds, per residue atomic fluctuations and inter-atomic distances. H-bonds with a cutoff of 3.2- Å and 160°, which were present for

more than 5% of the total trajectory, were recorded. VMD was used to render videos of the simulations and PyMOL was used to generate representative figures (51, 52).

Table S1. List of specific interactions at Affimer proteins-protein interface seen in crystal structure 5ML9.

	FcγRIIIa		distance in Å	water	distance in Å	Affimer F4		
125	GLN	[Oε1]	2.7	--	--	55	HIS	[Nε2]
130	ARG	[O]	2.9	--	--	57	PHE	[N]
130	ARG	[Nε]	2.5	--	--	55	HIS	[O]
130	ARG	[Nε2]	3.1	11	2.9	54	GLU	[O]
131	LYS	[Nω2]	2.7	--	--	58	PRO	[O]
131	LYS	[Nω2]	2.7	--	--	60	THR	[Oγ1]
132	TYR	[N]	2.8	--	--	85	ASN	[Nδ2]
132	TYR	[N]	2.8	1	2.6	85	ASN	[N]
134	HIS	[N]	2.4	--	--	19	GLU	[Oε2]
134	HIS	[Nε2]	2.7	--	--	22	GLU	[Oε2]
135	HIS	[N]	3.1	--	--	19	GLU	[Oε2]
135	HIS	[Nε2]	2.5	--	--	22	GLU	[Oε2]
136	ASN	[O]	2.5	37	2.6	19	GLU	[N]
137	SER	[Oγ]	3.1	--	--	16	ASN	[Nδ2]
137	SER	[Oγ]	2.8	50	2.9	16	ASN	[Nδ2]
138	ASP	[N]	2.6	--	--	16	ASN	[Oδ1]
--	--	--	--	50	2.9	62	THR	[Oγ1]
--	--	--	--	50	2.7	49	GLU	[Oε2]

Table S2: Average B factor per chain of AfG3.

Chain	Average B
A	66.1
B	104.2
C	73.6
D	76.5
water	62.8
all	80.1

Table S3. Specific interactions at AfG3-FcγRIIIa interface seen in crystal structure 5MN2.

FcγRIIIa			distance in Å	water	distance in Å	Affimer protein G3		
17	TYR	[OH]	2.8	1	2.8	85	HIS	[O]
83	GLN	[Nε2]	2.7	--	--	83	GLN	[O]
83	GLN	[Oε1]	2.6	2	2.9	83	GLN	[N]
85	GLU	[Oε2]	2.8	--	--	85	HIS	[N]
85	GLU	[Oε2]	2.6	1	--	--	--	--
86	VAL	[N]	3.2	37	3	85	HIS	[Nε2]
99	VAL	[N]	3.2	--	--	51	GLY	[O]
167	THR	[Oγ1]	3.4	--	--	86	ASN	[Nδ2]
169	ASN	[N]	3.1	--	--	83	GLN	[Oε1]
169	ASN	[O]	2.9	--	--	83	GLN	[Nε2]
--	--	--	--	2	2.9	83	GLN	[O]
--	--	--	--	2	2.8	52	PHE	[O]
--	--	--	--	2	3.0	98	TRP	[Nε]
--	--	--	--	37	3	86	VAL	[O]

		FcγRIIIa-AfG3			FcγRIIIb NA2-AfG3		
Donor residue	**Acceptor residue**	**Occupancy (%)**	**Avg Dist (Å)**	**Avg Angle (°)**	**Fraction of simulation**	**Average distance**	**Average angle**
Inter-molecular H-bonds							
FcγR-Trp98 (N)	AdG3-Gly52 (O)	26.14	2.91	159.11	15.92	2.85	151.78
FcγR-Val99 (N)	AdG3-Gly52 (O)	44.22	2.89	161.24			
FcγR-Arg18 (NH1/NH2)	AdG3-Asn86 (OD1)	39.30	2.84	152.25			
Intra-molecular H-bonds							
Gln94 (NE2)	Arg/Ser18 (O)	69.53	2.85	162.62	26.38	2.76	157.72
Glu21 (H)	Arg/Ser18 (O)				37.44	2.88	154.16
Leu20 (H)	Arg/Ser18 (O)				57.48	2.85	159.65
Arg/Ser18 (H)	Ala95 (O)	32.87	2.87	151.96			
Arg18 (NH1/NH2)	Glu166 (OE2)	35.71	2.81	151.90			
Arg18 (NH1/NH2)	Glu166 (OE1)	19.15	2.81	151.57			
Trp98 (HE2)	Gln83 (OE1)	38.31	2.84	156.71			

Table S4. Selected H-bond distances in the key interactions between FcγRIIIa/b and AfG3 in molecular dynamics simulations.

Table S5: Protein/Affimer protein crystallization conditions.

Protein	Affimer protein	Screen	Conditions
FcγRIIIa 158F	AfG3	JCGS+ (D12)	20.0% v/v glycerol 16.0% w/v polyethylene glycol 8000 0.04 M potassium di-hydrogen phosphate
FcγRIIIa 158V	AfF4	JCSG+ (E2)	2.0 M ammonium sSulphate 0.1 M sodium cacodylate pH=6.50 0.2 M sodium chloride

Table S6: List of sugar-modified residues.

FcγRIIIa-AfG3	**FcγRIIIa-AfF4**
A Asn38	A Asn45
A Asn45	A Asn74
A Asn74	A Asn169
A Asn162	
A Asn169	
B Asn45	
B Asn74	

Table S7: Cloning primer sequences.

Primer name	Vector / Fragment	Size (bp)	Sequence (5'-3')
FCGR2A ectoF	pOPINTTG 2Aectodomain	551	GCGTAGCTGAAACCGGCGCTCCCCCAAAGGCTGTGC
FCGR2A ectoR			GTGATGGTGATGTTTGCTGGGCACTTGGACAGTGATGG
FCGR2A SDMF	pOPINTTG 2Aectodomain 131R	551	TCCCAGAAATTCTCCCGTTTGGATCCCACCTTC
FCGR2A SDMR			GAAGGTGGGATCCAAACGGGATTTCTGGGA
FCGR3A ectoF	pOPINTTG 3A ectodomain	551	GCGTAGCTGAAACCGGCGAAGATCTCCCAAAGGCTGTGGTG
FCGR3A ectoR			GTGATGGTGATGTTTACCTTGAGTGATGGTGATGTTCACAG
pFBHYGFCGR2AF	pFBHYGSNAP 2A full length	986	AATTGTCGACGAATTCATGACTATGGAGACCCAAATGTC
FCGR2A SNAPR			CTTTGTCCATGGATCCGTTATTACTGTTGACATGGTC
pFBHYGFCGR3AF	pFBHYGSNAP 3A full length	905	AATTGTCGACGAATTCATGGGTGGAGGGGCTGGGGAA
FCGR3A SNAPR			CTTTGTCCATGGATCCTTTGTCAGGGTCTTTTCTCCA
FCGR3ASDMf	pFBHYGSNAP 3A full length 158V	905	CTTCTGCAGGGGGCTCTTGTTGGGAGTAAAAATGT
FCGR3ASDMr			ACATTTTTACTCCCAACAAGCCCCCTGCAGAAG
pFBHYGFCGR3AF	pFBHYG 3B full length	842	AATTGTCGACGAATTCATGGGTGGAGGGGCTGGGGAA
FCGR3B R			GCCGCTCGAGGATCCTCAAATGTTTGTCTTCACAGAG

Supplementary Figure Legends

Figure S1. FcγRIIIa interactions with AfF4 and AfG3 (123nM-10μM) by surface plasmon resonance. (**a**) Amine coupled receptors. Single cycle kinetics 1:1 binding model (superimposed red line) provided kinetic measurements of association (k_a) and dissociation (k_d) and equilibrium dissociation constant (K_D) as indicated. Interaction kinetics exceeded the measurement capabilities of the instrument at higher Affimer protein concentrations. (**b**) Orientated C-terminal Avitag-immobilised receptors. Steady-state affinity measurements from SPR for each Affimer protein interaction with immobilised fully glycosylated and Endo F1-treated FcγRIIIa.

Figure S2. Overlapping binding sites on FcγRIIIa for IgG Fc and AfF4. FcγRIIIa-IgG Fc from PDB ID code 3SGJ (yellow) and -AfF4 from PDB ID code 5ML9 (red) interfaces overlap by ~50% (orange) illustrating the steric nature of the IgG inhibition. Interface surface areas were calculated using PISA (EMBL-EBI).

Figure S3. Per-residue Root Mean Square Deviation (RMSD) analysis of FcγRIIIa/b-AfF4 and -AfG3 molecular dynamics trajectories. RMSD values were averaged over

three repeats and show that all simulations remained stable during the timescale of the simulations, and that 200ns was sufficient for the RMSD to converge to a stable value.

Figure S4. Atomic fluctuation by residue of FcγRIIIa/b-AfF4 and –AfG3 molecular dynamics trajectories. Higher values represent greater fluctuation. All values were averaged over three repeats. Purple plots represent FcγRIIIa-containing simulations and green plots represent FcγRIIIb-containing simulations.

Figure S5. Molecular dynamics simulations suggest proposed mechanism of AfG3-mediated FcγRIIIa inter-domain angle restriction. (a) View of D1-D2 interdomain hinge in FcγRIIIa and FcγRIIIb after 200ns of molecular dynamics simulation, D1 depicted in aqua marine, D2 depicted in wheat. **(b)** Measurements *i* and *ii* describe interatomic distances over the course of the 200ns AfG3 simulations for both FcγRIIIa (purple lines) and FcγRIIIb (green lines) averaged over three repeats. Formation of the γaArg18-γaGln94 H-bond early in the simulations leads to formation of an additional interdomain H-bond between γaGln83 and γaTrp99. In FcγRIIIb the lack of *i* formation leads to greater flexibility between D1 and D2 preventing the formation of *ii*.

Figure S6. Stereo image of AfF4-FcγRIIIa ectodomain model fitted to electron density map contoured at 2.0 sigma. FcγRIIIa in purple stick and AdF4 in orange stick representation.

Fig.1

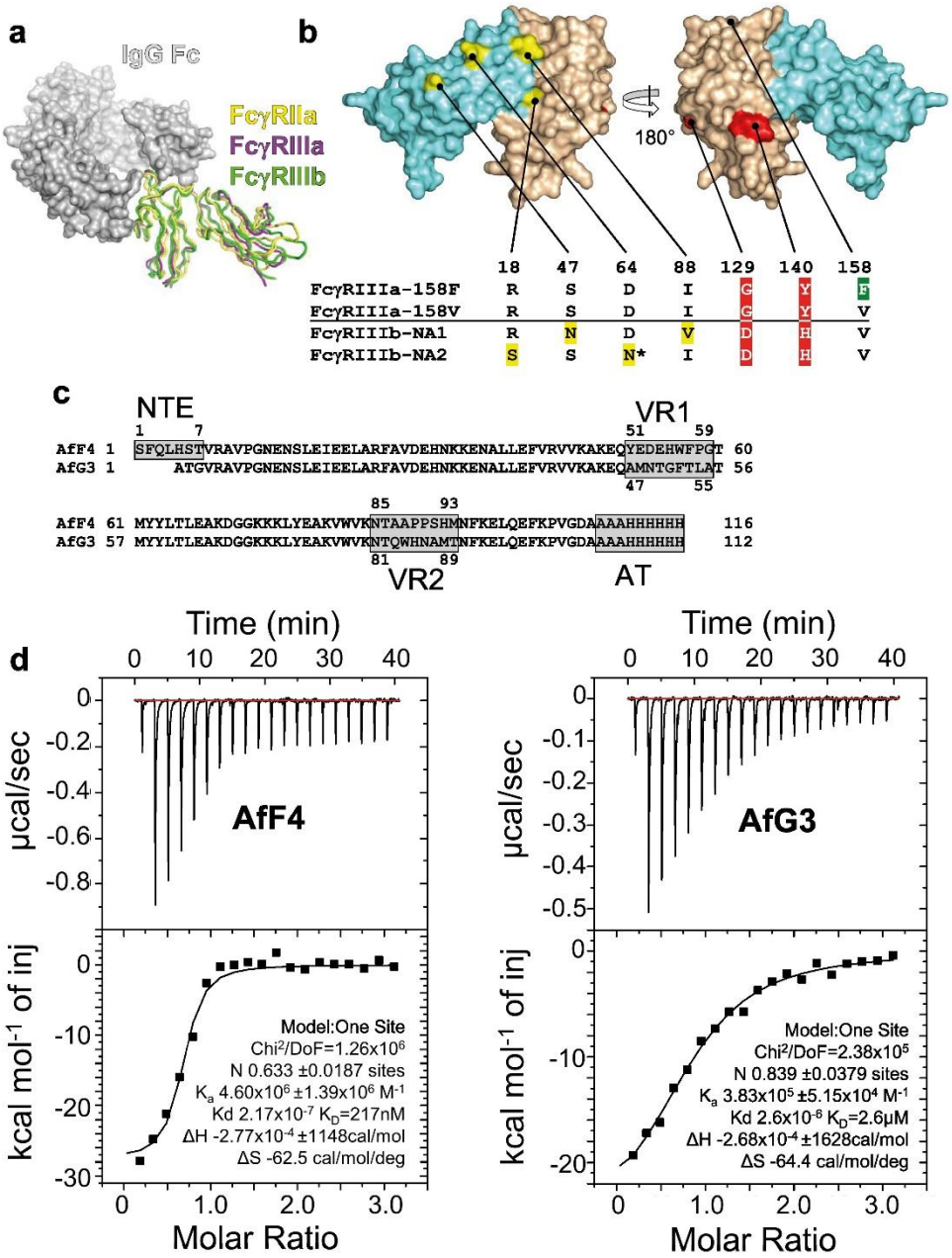
a
IgG Fc
FcγRIIa
FcγRIIIa
FcγRIIIb
b
180°
18 47 64 88 129 140 158
FcγRIIIa-158F R S D I G Y F
FcγRIIIa-158V R S D I G Y V
FcγRIIIb-NA1 R N D V D H V
FcγRIIIb-NA2 S S N* I D H V
c
NTE
VR1
VR2
AT
AfF4 1 SFQLHSTVRAVPGNENSLEIEELARFAVDEHNKKENALLEFVRVVKAKEQYEDEHWFPGT 60
AfG3 1 ATGVRAVPGNENSLEIEELARFAVDEHNKKENALLEFVRVVKAKEQAMNTGFTLAT 56
AfF4 61 MYYLTLEAKDGGKKKLYEAKVWVKNTAAPPSHMNFKELQEFKPVGDAAAAHHHHH 116
AfG3 57 MYYLTLEAKDGGKKKLYEAKVWVKNTQWHNAMTNFKELQEFKPVGDAAAAHHHHH 112
d
Time (min)
µcal/sec
kcal mol-1 of inj
Molar Ratio
AfF4
Model:One Site
Chi2/DoF=1.26x10^6
N 0.633 ±0.0187 sites
Ka 4.60x10^6 ±1.39x10^6 M-1
Kd 2.17x10-7 KD=217nM
ΔH -2.77x10-4 ±1148cal/mol
ΔS -62.5 cal/mol/deg
AfG3
Model:One Site
Chi2/DoF=2.38x10^5
N 0.839 ±0.0379 sites
Ka 3.83x10^5 ±5.15x10^4 M-1
Kd 2.6x10-6 KD=2.6µM
ΔH -2.68x10-4 ±1628cal/mol
ΔS -64.4 cal/mol/deg

Fig. 2.

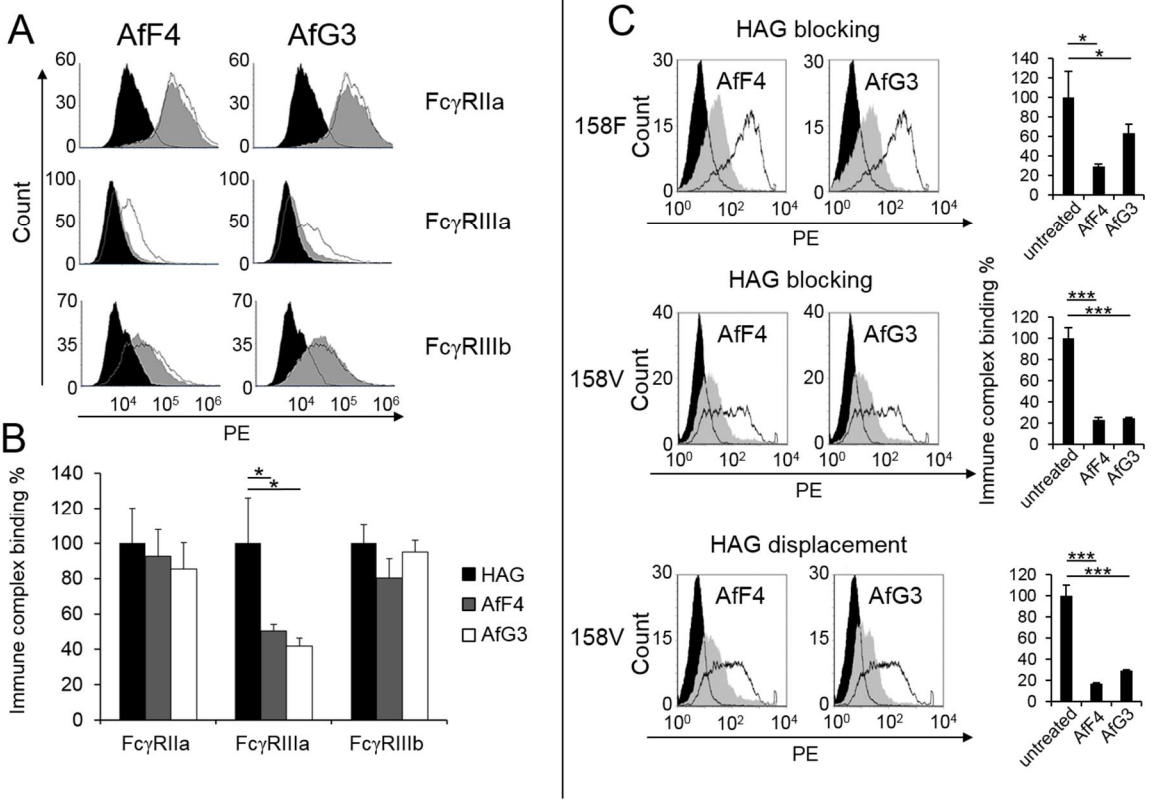
A
AfF4
AfG3
FcγRIIa
FcγRIIIa
FcγRIIIb
Count
PE
B
Immune complex binding %
HAG
AfF4
AfG3
FcγRIIa
FcγRIIIa
FcγRIIIb
C
HAG blocking
158F
HAG blocking
158V
HAG displacement
158V
Count
PE
Immune complex binding %
untreated
AfF4
AfG3

Fig. 3.

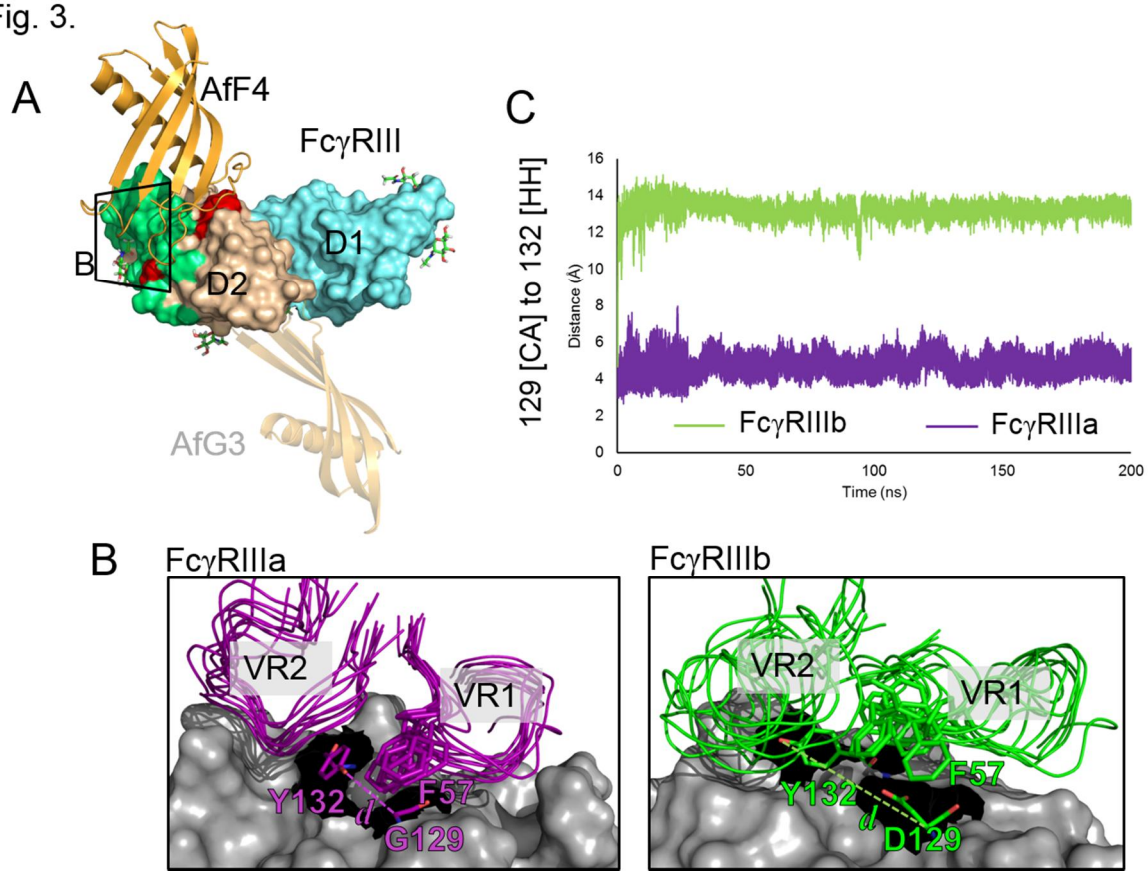
A
AfF4
FcγRIII
B
D1
D2
AfG3
C
129 [CA] to 132 [HH]
Distance (Å)
FcγRIIIb
FcγRIIIa
Time (ns)
B
FcγRIIIa
FcγRIIIb
VR2
VR1
Y132
F57
G129
D129

Fig. 4.

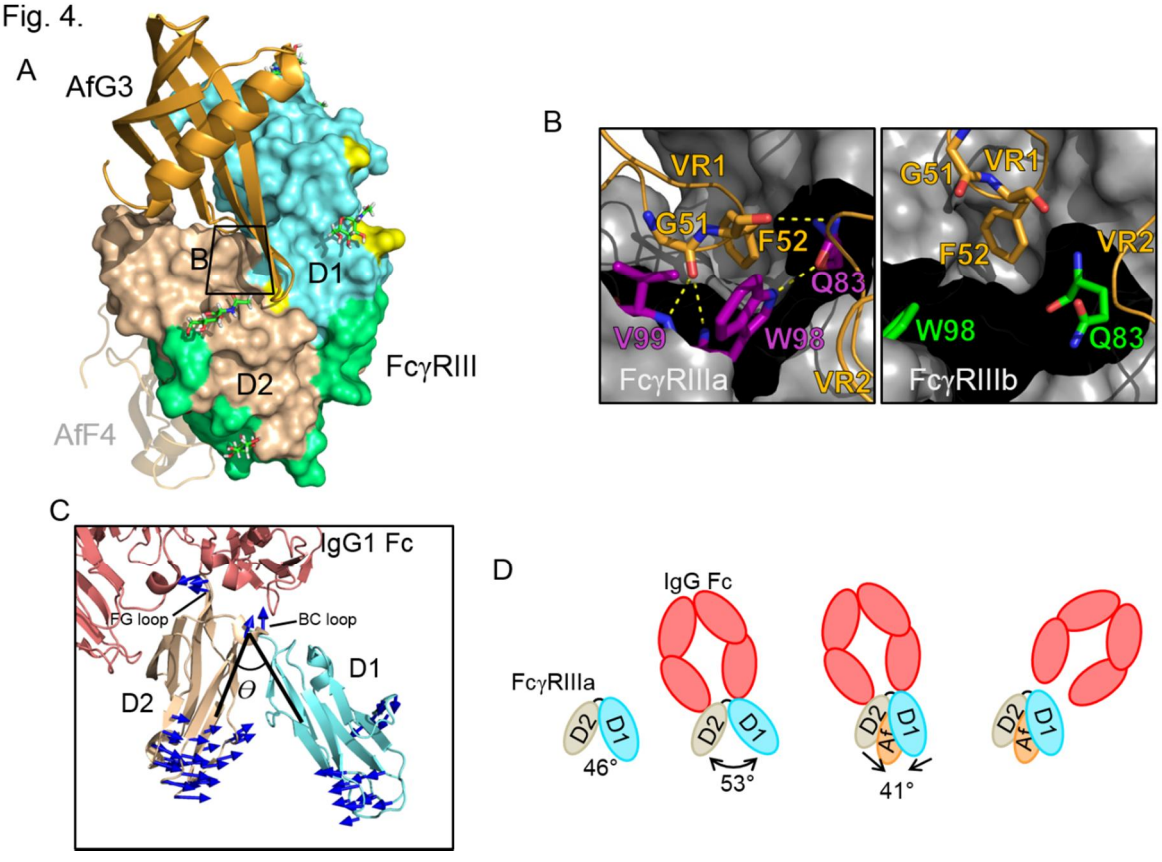
A
AfG3
B
D1
D2
FcγRIII
AfF4
B
VR1
G51
F52
Q83
V99
W98
FcγRIIIa
VR2
FcγRIIIb
C
IgG1 Fc
FG loop
BC loop
D1
D2
θ
D
IgG Fc
FcγRIIIa
46°
53°
41°

Fig. 5.

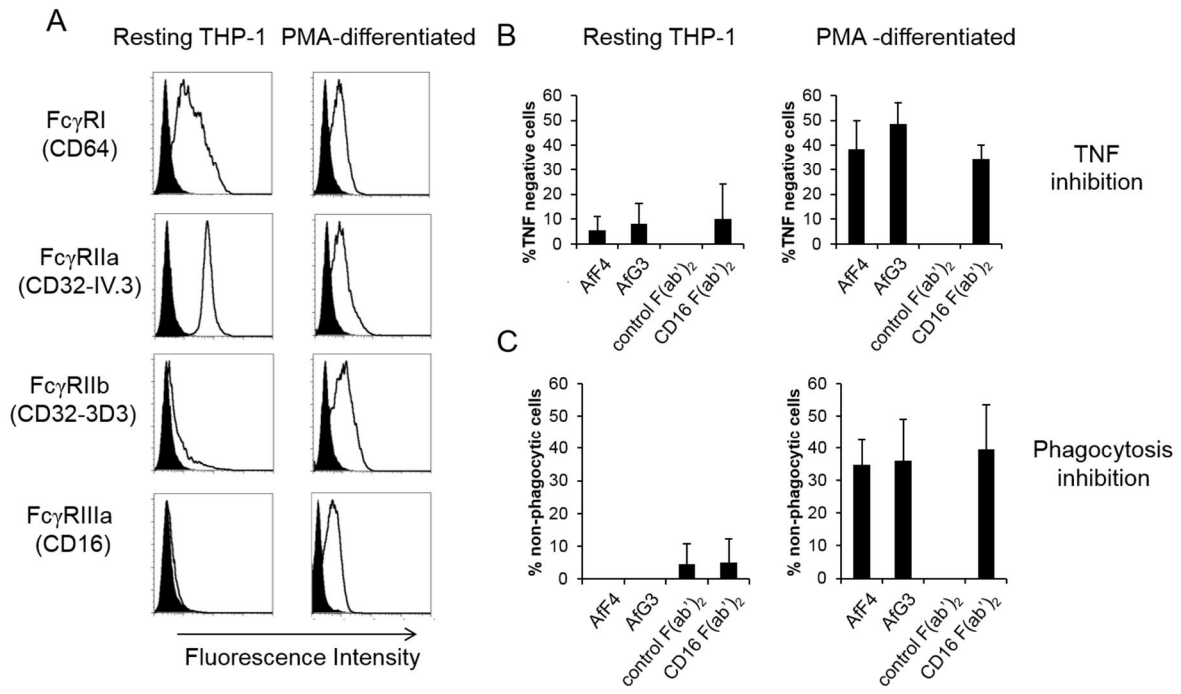
A
Resting THP-1
PMA-differentiated
FcγRI (CD64)
FcγRIIa (CD32-IV.3)
FcγRIIb (CD32-3D3)
FcγRIIIa (CD16)
Fluorescence Intensity
B
Resting THP-1
PMA -differentiated
% TNF negative cells
AfF4
AfG3
control F(ab')2
CD16 F(ab')2
TNF inhibition
C
% non-phagocytic cells
Phagocytosis inhibition

Fig. S1.

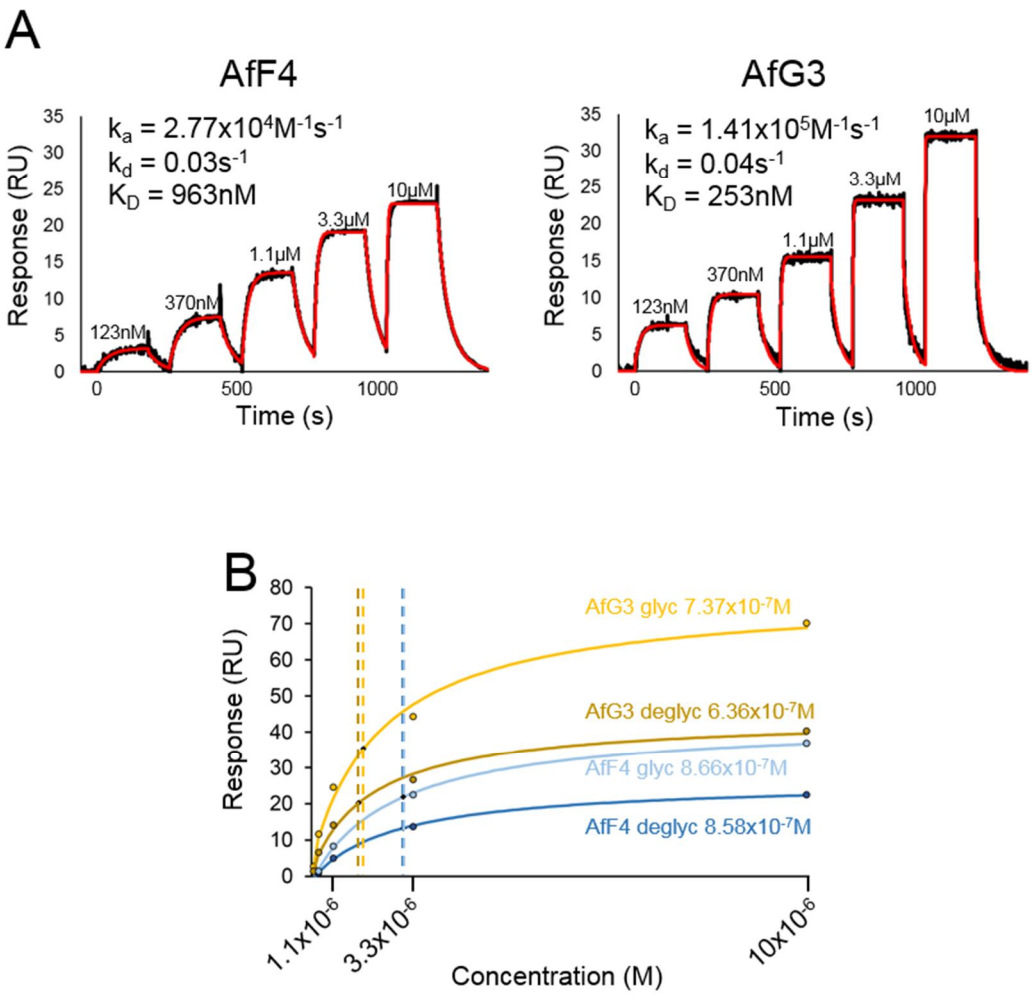
A
AfF4
k_a = 2.77x10^{4}M^{-1}s^{-1}
k_d = 0.03s^{-1}
K_D = 963nM
123nM
370nM
1.1µM
3.3µM
10µM
Response (RU)
Time (s)
AfG3
k_a = 1.41x10^{5}M^{-1}s^{-1}
k_d = 0.04s^{-1}
K_D = 253nM
123nM
370nM
1.1µM
3.3µM
10µM
Response (RU)
Time (s)
B
AfG3 glyc 7.37x10^{-7}M
AfG3 deglyc 6.36x10^{-7}M
AfF4 glyc 8.66x10^{-7}M
AfF4 deglyc 8.58x10^{-7}M
Response (RU)
1.1x10^{-6}
3.3x10^{-6}
10x10^{-6}
Concentration (M)

Fig. S2.

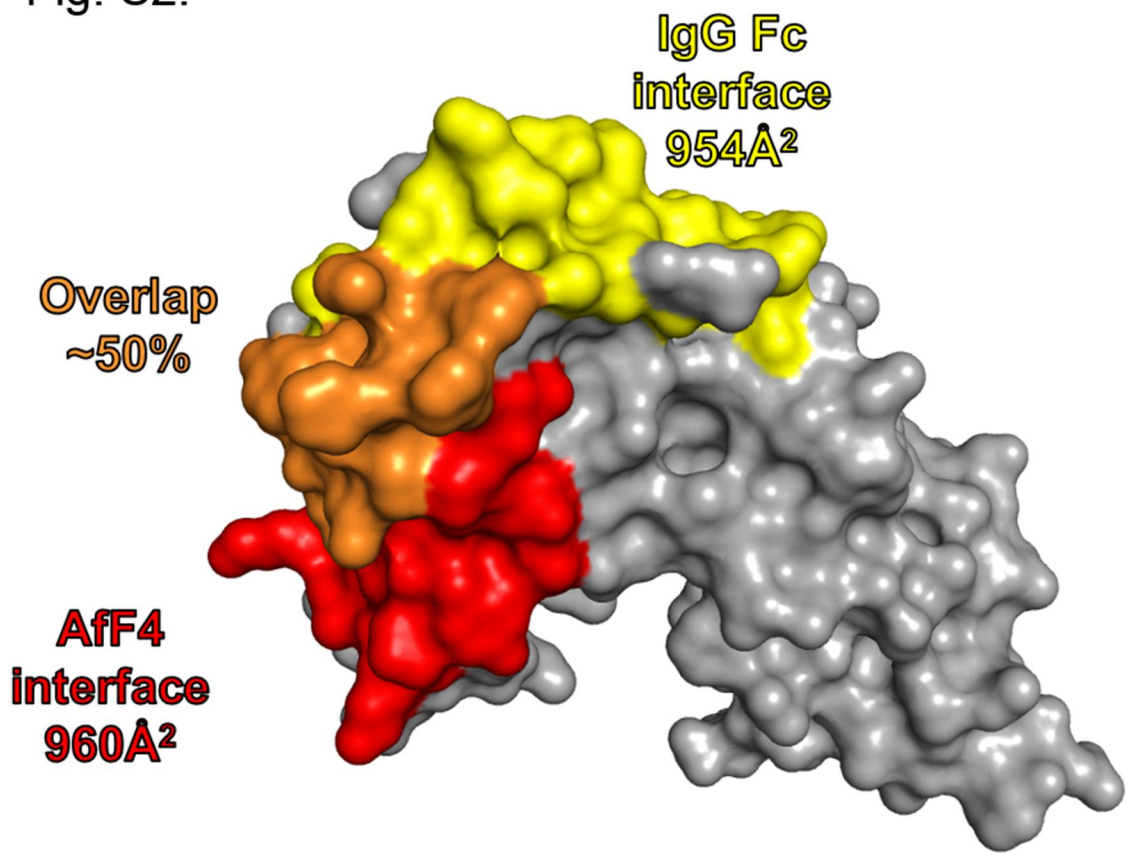
IgG Fc
interface
954Å²
Overlap
~50%
AfF4
interface
960Å²

Fig. S3.

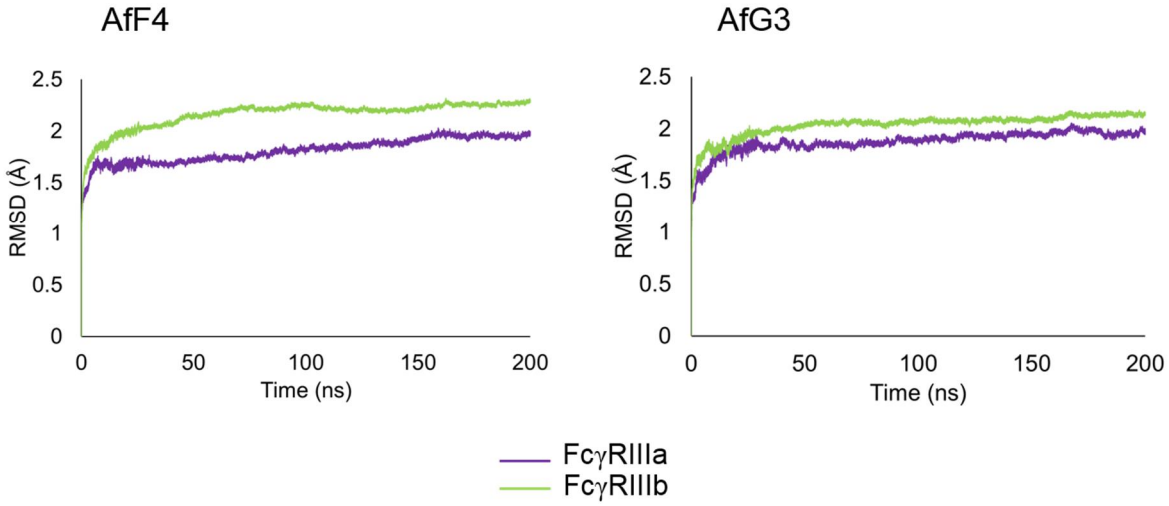
AfF4
AfG3
RMSD (Å)
Time (ns)
0
0.5
1
1.5
2
2.5
0
50
100
150
200
FcγRIIIa
FcγRIIIb

Fig. S4.

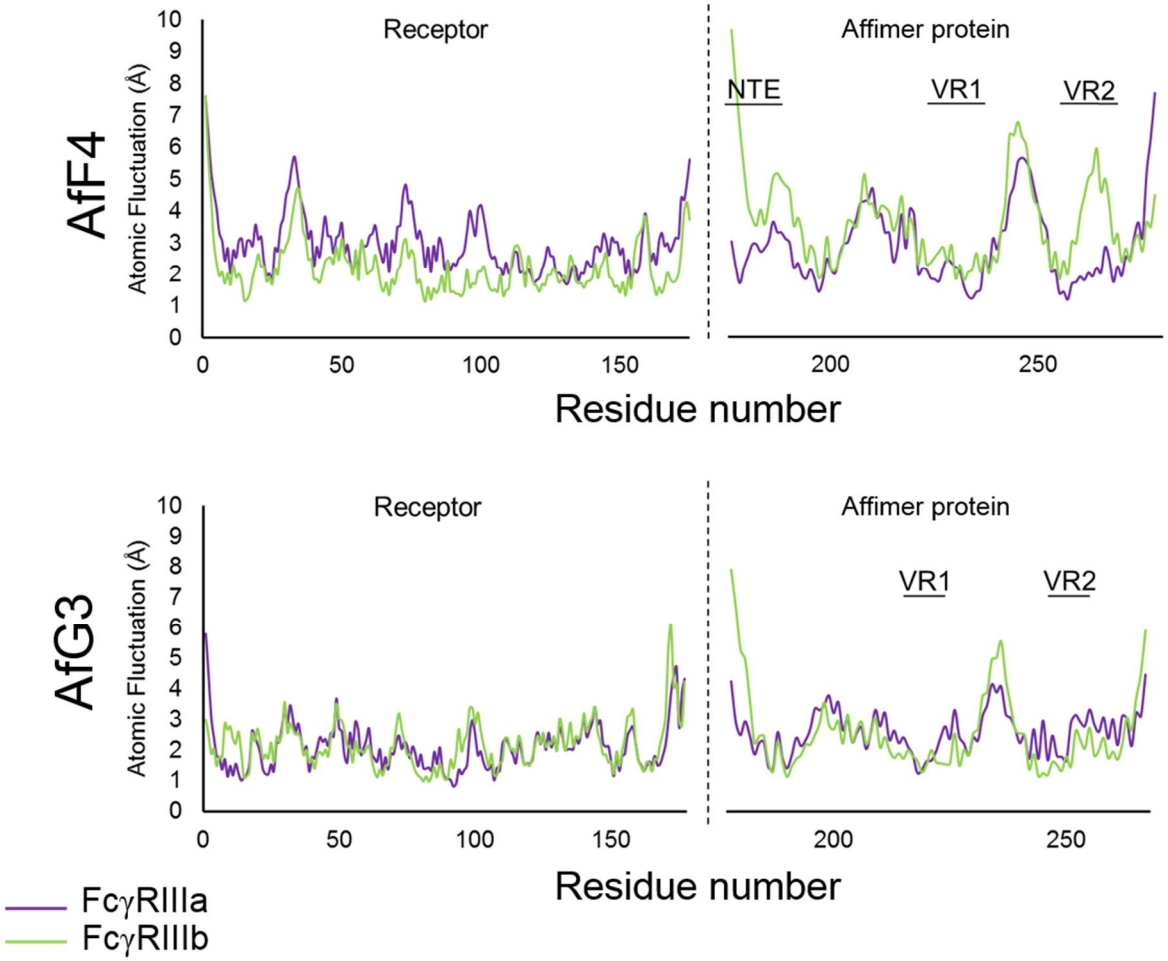
AfF4
Atomic Fluctuation (Å)
Receptor
Affimer protein
NTE
VR1
VR2
Residue number
AfG3
Atomic Fluctuation (Å)
Receptor
Affimer protein
VR1
VR2
Residue number
FcγRIIIa
FcγRIIIb

Fig. S5.

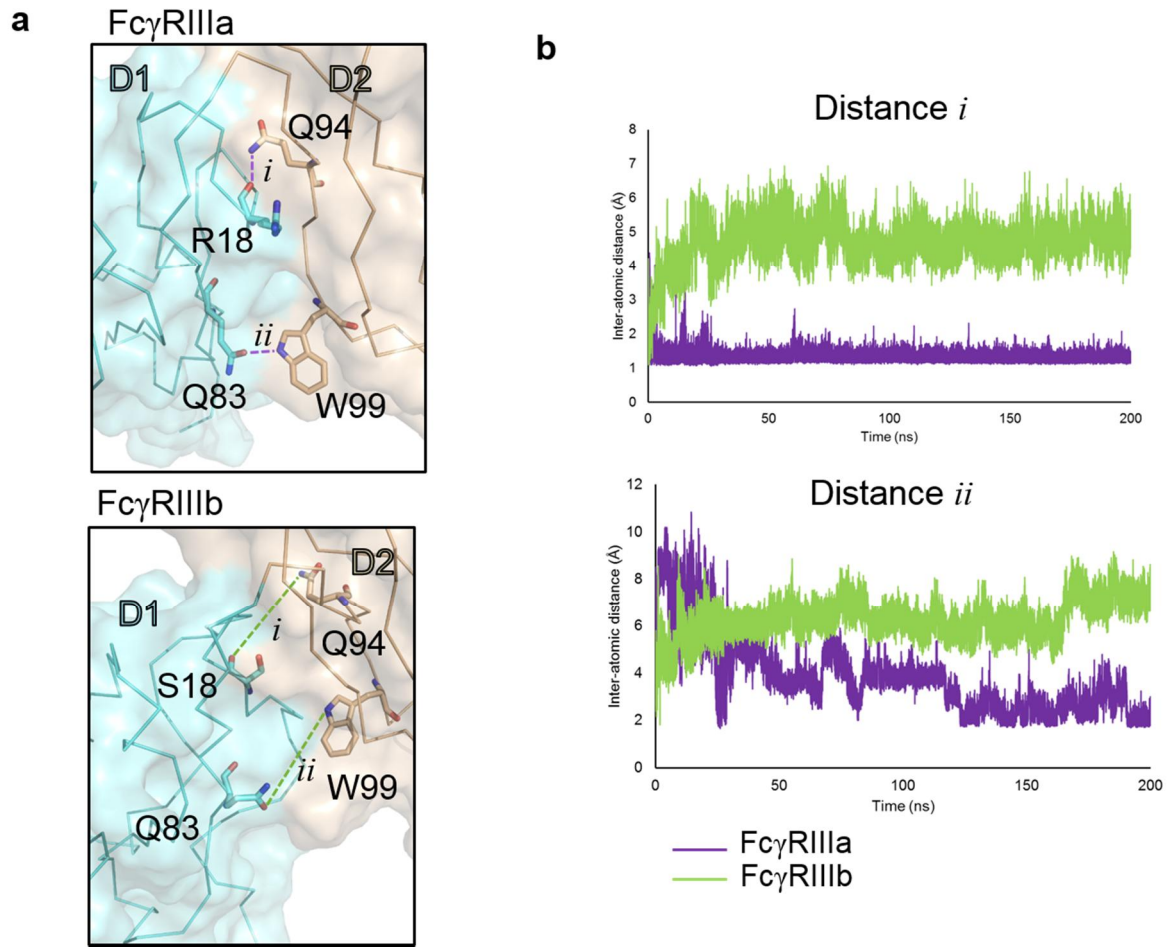
a
FcγRIIIa
D1
D2
Q94
i
R18
ii
Q83
W99
FcγRIIIb
D1
D2
i
Q94
S18
ii
W99
Q83
b
Distance i
Inter-atomic distance (Å)
Time (ns)
Distance ii
Inter-atomic distance (Å)
Time (ns)
FcγRIIIa
FcγRIIIb

Fig. S6.

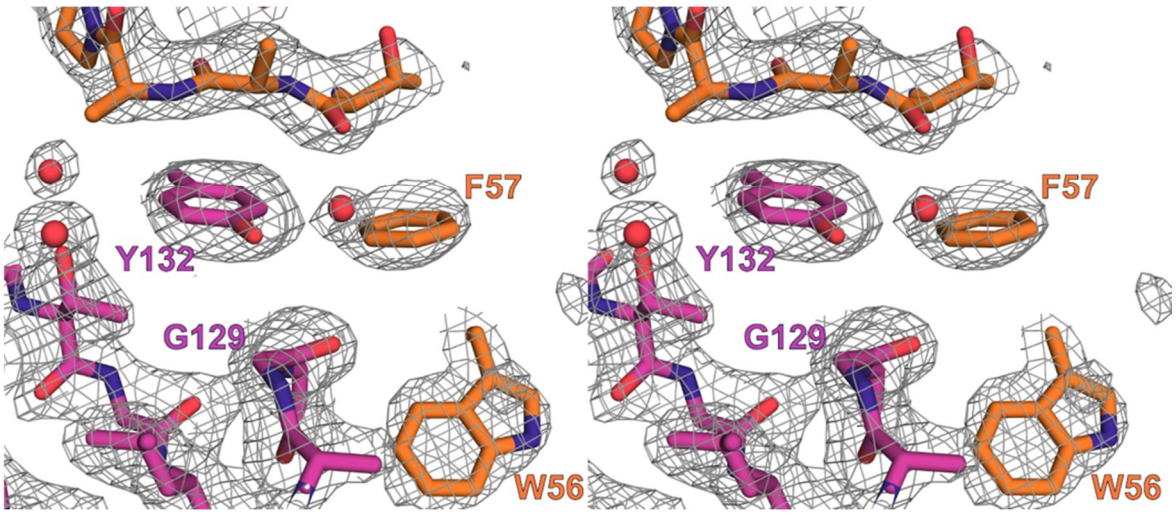
F57
Y132
G129
W56
F57
Y132
G129
W56